

---

## 2 Atomic Force Microscopy in Practice

### Abstract

Imaging with an AFM requires an appropriate preparation of the sample as well as of the force microscope for the planned experiment. In this chapter, the basic steps to prepare an AFM setup for a standard contact mode and for intermittent contact (tapping) mode AFM operation will be briefly treated. In addition, practical hints regarding the selection of probes tips, sample preparation, choice of operation modes, and imaging media are provided. Finally, tip modification procedures, calibration issues (spring constant, scanner, photodetector, etc.), general guidelines for AFM laboratories, as well as data evaluation and handling will be very briefly treated.

### 2.1 Assembling of AFMs for Operation

Assembling different brands and types of force microscopes requires naturally instrument and mode-specific steps and may differ in particular details due to practical peculiarities. On the basis of two common AFM modes, a scanned sample AFM (such as a Digital Instruments/VEECO multimode) and a tip scanning stand alone AFM (such as a Molecular Imaging Pico SPM), the overall principles and basic steps will be introduced in this chapter. These can be generalized to within the limitations of the particular type of AFM the reader is using. We recommend strongly to consult the corresponding manuals.

#### 2.1.1 Scanned Sample AFM (Contact Mode)

The typical scanned sample AFM scanning unit consists of the following parts: a base, a scanner, and an optical head, in which a holder for the cantilever is mounted (Fig. 2.1). In addition, a probe tip/cantilever and sample, which will be mounted on a metallic sample puck, are required. Careful handling of the sensitive equipment (avoid shock, mechanical stress on the cables, temperatures above 40°C, high humidity for the scanner, etc.) is a prerequisite for this work. We recommend wearing

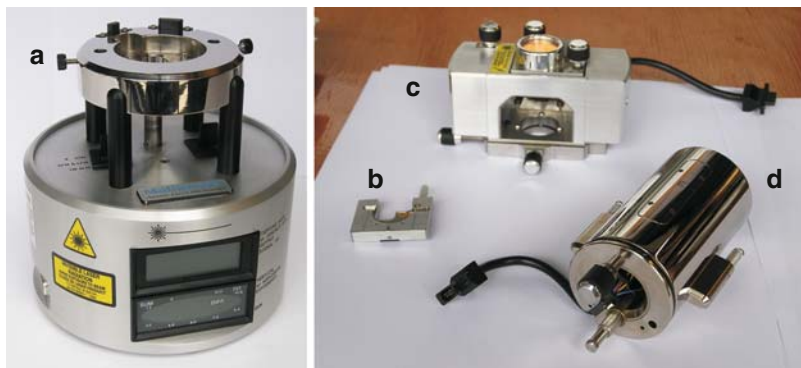


**Fig. 2.1** Photographs of the essential components of a sample scanning AFM: (a) scanner base, (b) cantilever holder, (c) optical head, and (d) scanner of a typical scanned sample AFM

typical unpowdered lab gloves (made from latex, polyurethane, etc.) to prevent possible contamination of the instrument and samples with fingerprints. In addition, we recommend consulting the manuals for risks of electric shock if cables are not properly used, if there is exposure to laser light, etc., as applicable.

The sample (mounted on a metallic sample puck) is attached to the scanner, which will later position the sample in all three spatial directions. The optical head comprises the cantilever–tip assembly in a special holder, as well as the optics (laser and photodetector) of the beam-deflection detection scheme. The base contains electronic circuitry and is the interface between controller and actual force microscope. It also serves as physical holder for the scanner and may include a stepper motor, which is used for the coarse and fine approach between tip and sample (see below).

The manual assembly can be divided into four basic steps:

*Route (a)*

1. Mounting of the cantilever in its holder
2. Mounting of the scanner on the base
3. Securing the cantilever holder in the optical head
4. Mounting of the optical head/cantilever holder assembly to the scanner

Alternatively, one can follow

*Route (b)*

1. Mounting of the cantilever in its holder
2. Mounting of the scanner on the base
3. Mounting of the optical head to the scanner
4. Securing the cantilever holder in the optical head

These steps are identical for contact mode (CM) and intermittent contact (tapping) mode operation, except for the choice of the cantilever. As discussed in more detail below (Sect. 2.2), CM levers for experiments in ambient conditions are relatively soft (with a cantilever spring constant  $k_c$  between  $\sim 0.05$  and  $\sim 1.00$  N/m), while tapping mode probes are stiffer ( $k_c \sim 10$ – $100$  N/m). For tapping mode operation in liquids, such as water, CM levers are used.

First, the cantilever is mounted in its holder. Care has to be taken to hold the cantilever chip gently with the tweezers on the side, as shown schematically by the arrows in Fig. 2.2a). Contact of the tweezers with the lever (and potentially the tip) must be avoided; in addition, the chip should always reside with its bottom part on the sample preparation table. If the chip flips over (e.g., because it has been dropped while handling it with the tweezers), one has to assume that the tip may be damaged,

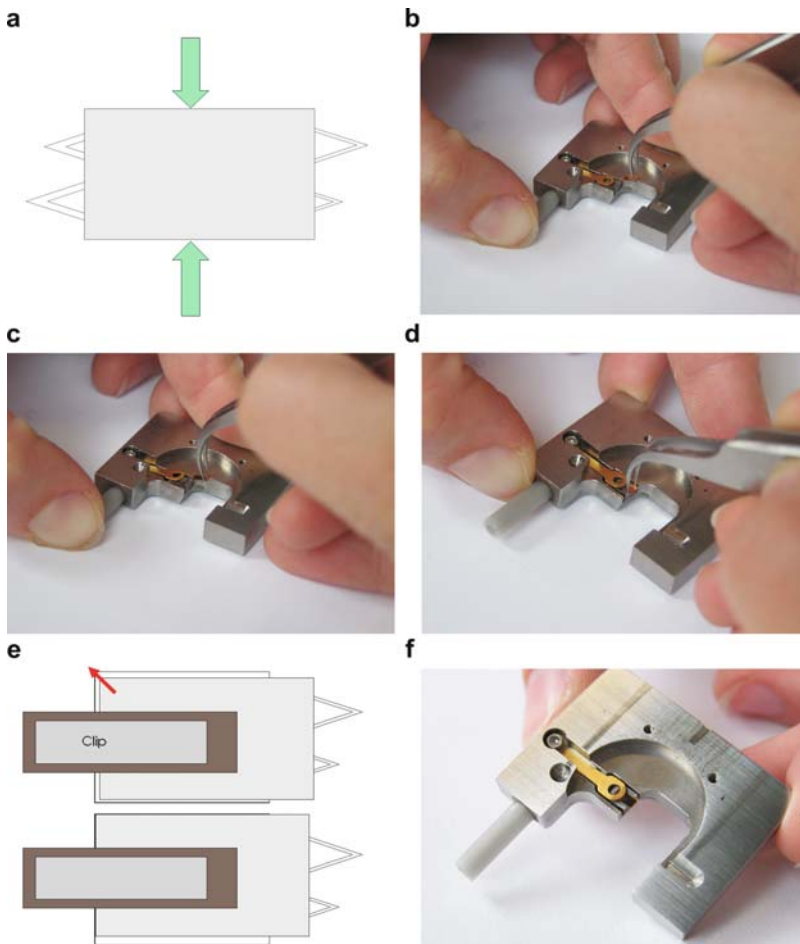


**Fig. 2.2** Stepwise mounting of the cantilever into the cantilever holder (details: see text)

even though the cantilever may still be visibly unimpaired (as viewed, e.g., through an eyepiece or an optical microscope).

To open the brass clip of the cantilever holder, the holder is pressed against the table. Then the chip is slid carefully under the clip and the load is released. One should gently push the chip to the end of the “mold,” preferably in plane-parallel contact with the sidewall, to avoid possible movement at a later stage.

To start the assembly of the AFM head, the safety screw on the scanner is removed (Fig. 2.3a) and the scanner is mounted carefully on the base (Fig. 2.3b). The stepper motor is slowly moved “up” (using the toggle switch, Fig. 2.3c) to make sure that the hexagonally shaped screw and the fitting on the base match.

Once the scanner sits tightly on the base, it is secured by inserting the safety screw from below (Fig. 2.4a). Subsequently, the scanner cable is carefully inserted into the corresponding plug on the base (Fig. 2.4b).

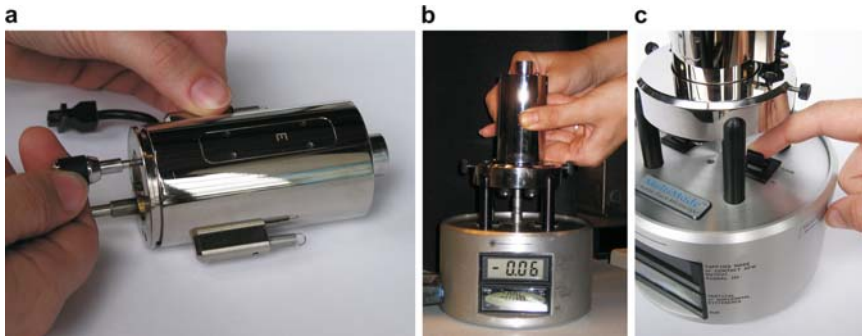


**Fig. 2.3** Stepwise mounting of piezo scanner: (a) removal of the safety screw; (b) placement of scanner on the base; (c) operation of the stepper motor (details: see text)

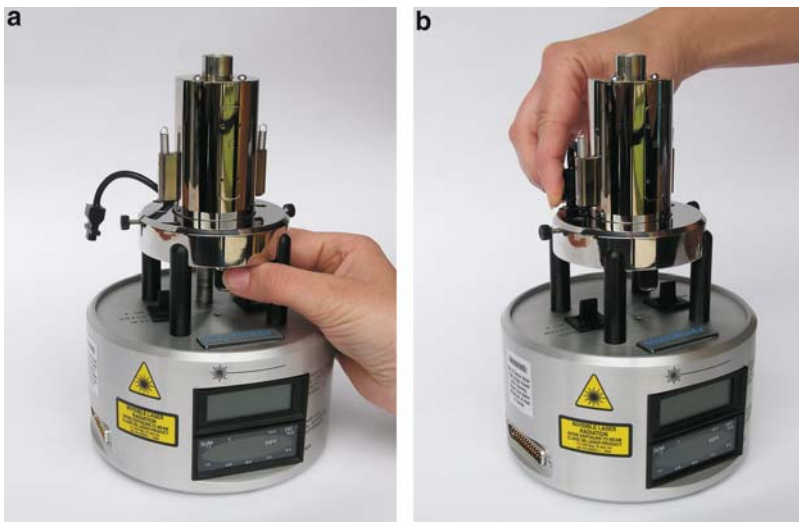


**Fig. 2.4** (a) Securing the scanner's safety screw; (b) insertion of scanner cable into base

To mount the optical head onto the scanner/base assembly, there are two alternative options:

One can (1) first mount the head, followed by insertion of the cantilever holder and securing the cantilever holder screw on the backside (*Route b*, Fig. 2.5), or (2) vice versa, i.e., the holder is secured before the head is mounted (*Route a*, Fig. 2.6). In both cases, the head should be lowered carefully onto the three metal balls on the scanner; holding the head tightly with one hand, the springs on both sides of the scanner are slid over the corresponding metal pins so that they securely hold the optical head in place. *Careful*: Hold the head tightly, especially if only one spring is attached and make sure that the springs are properly attached before release of the grip on the optical head. Otherwise, the head may fall off the scanner and will likely be damaged. Once the head is secured, the scanner cable should be inserted into the corresponding plug on the base.

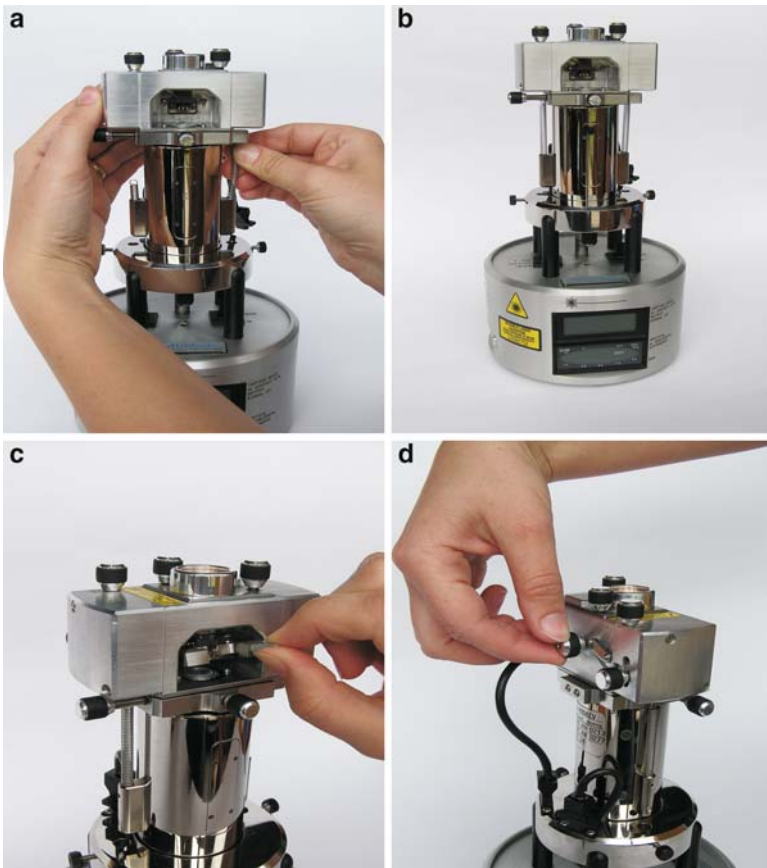


**Fig. 2.5** Essential steps of mounting the optical head: (a) Mounting of the optical head and securing of the springs; (b) optical head mounted on the scanner; (c) insertion of cantilever holder into optical head; (d) fixation of cantilever holder

Once the optical head, scanner, and base have been assembled and the cables of the scanner and the optical head have been attached, the base can be connected to the controller, following the specifications and instructions of the manufacturer. Care has to be taken that the controller is *not* running and is *not* sending high-voltage signals to the scanner.

To prepare the AFM setup for an experiment, the laser must be aligned, followed by the adjustment of the photodiode position, the mounting of the sample, and finally the crude and fine approach of the tip toward the sample surface.

The laser light position can be altered by turning the screws of the laser stage (Fig. 2.7). To detect where the laser light is being focused and where the reflected beam is directed to, a piece of paper can be inserted into the path of the beam (see

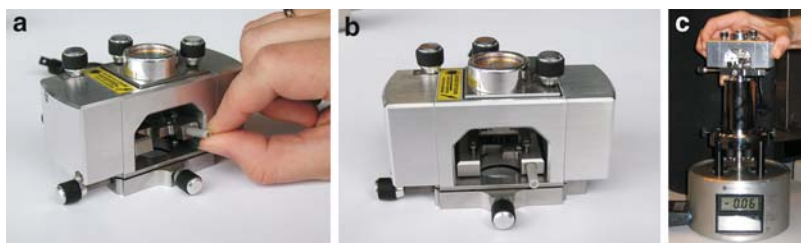


**Fig. 2.6** (a) Insertion of cantilever holder; (b) premounted cantilever holder (the holder has been fixed by tightening the corresponding screws, compare Fig. 2.5d); (c) mounting of cantilever holder/optical head assembly onto the scanner

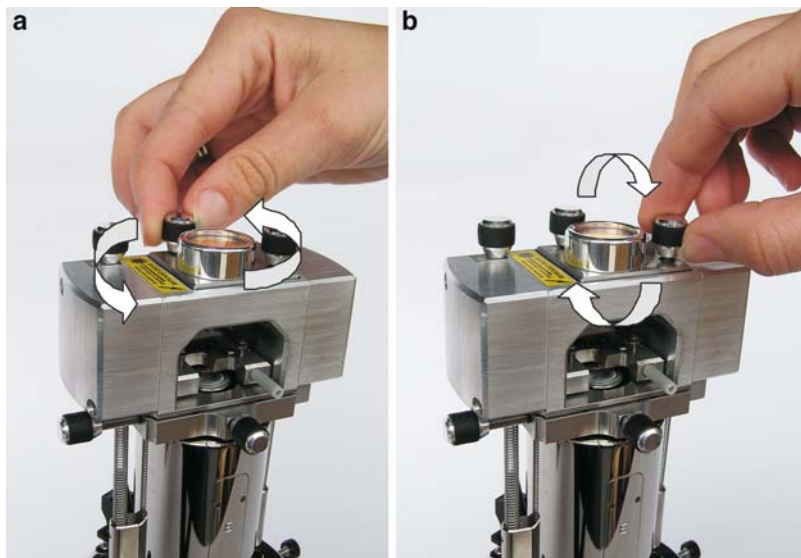


**Fig. 2.7** Adjustment of laser light position and alignment via laser stage screws

below). However, please be careful: do not touch the mirror; also never insert reflective objects such as tweezers into the optical path, as laser light may be reflected into the unprotected eye.

An alternative method is to hold the head firmly in one hand and to guide the laser light onto a piece of paper on the table. For this, the head must be detached from the base by carefully removing the springs that secure the head (see above). Instead of analyzing the reflected light from the cantilever, which reaches the photodiode, the blocking of the incident beam is monitored.

The laser light is first directed downward onto the metallic top of the piezo scanner. The laser is reflected and scattered on the rough metal surface, which is easily detected by the eye. As shown schematically in Fig. 2.8a, the laser light spot discernible on the metal is moved to the right using the screws on the laser stage. Once the laser light hits the cantilever substrate, the intense spot on the metal due to reflection/scattering is no longer visible. Subsequently, the laser stage is moved in the opposite direction (corresponding to a movement of the laser spot to the left) such that the laser spot becomes detectable again. This means that the laser light is reflected at a position indicated by the faint spot in Fig. 2.8a, i.e., somewhere on the vertical (dashed) line.

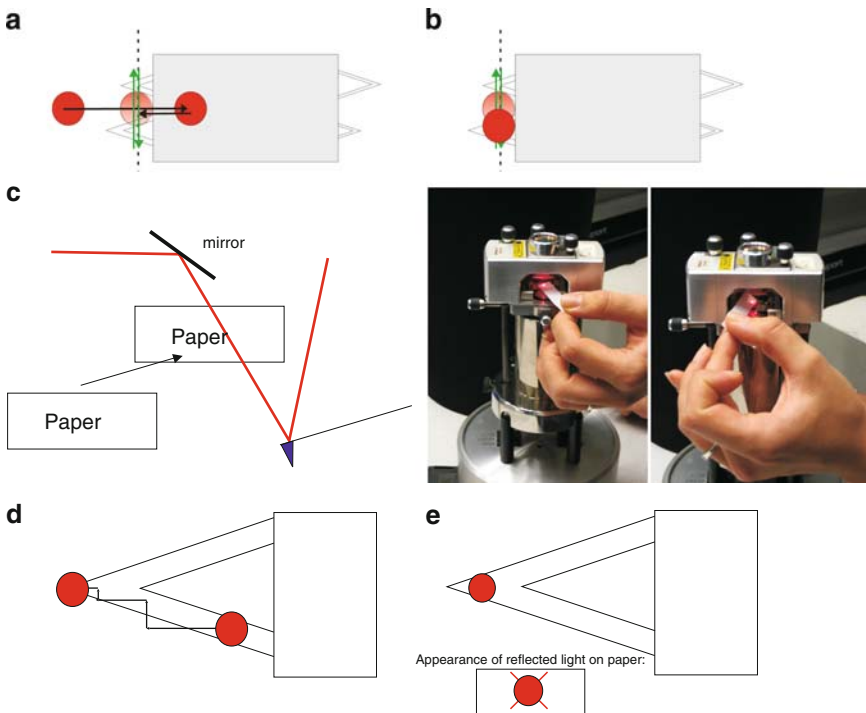


**Fig. 2.8** Stepwise process of laser alignment using the paper method (details: see text)

Now we move the spot (using the laser stage) up and down (Fig. 2.8b). If the laser light is reflected off the cantilever, the intensity of the light reflected from the metal is reduced, which can be seen again easily by bare eye. The part of the reflected intensity that is missing is directed toward the mirror and the photodiode (Fig. 2.8c). As mentioned, the reflected beam can be detected conveniently using a piece of paper.

The aim of the paper insertion is to detect the light reflected off the cantilever, as shown below. To properly position the paper to be able to detect the reflected laser light, the piece of paper is first moved into the incident beam. A sharp laser light spot can be easily detected. Subsequently, the paper is moved to the left into a position where the incident light is no longer blocked by the paper. If the alignment procedure according to Fig. 2.8a, b has been successfully carried out, we can observe the reflected laser light as a spot on the paper once we unblock the incident beam.

Having located the reflected laser light, we move the spot in an iterative manner to the end of the cantilever (shown in Fig. 2.8d). While we monitor the reflected laser light on the paper, the spot is moved using the laser stage to the left hand side. If the intensity decreases, the laser stage is moved in the vertical direction (up or down, as required). Continued movement to the left and correction in the vertical direction will ultimately result in a laser spot position on the very end of the cantilever. Reflection from the cantilever edges may result in the appearance of the spot with two diagonal lines, as shown in Fig. 2.8e. For optimized imaging, the spot is moved slightly to the right to ensure a spot on the paper with a well-defined appearance that is devoid of any stray light.

After aligning the laser, the mirror position is turned such that the reflected laser light is directed onto the photodiode (Fig. 2.10a). A maximized sum signal shows a good position (Fig. 2.9). Subsequently, the spot is centered on the photodiode by moving the diode in the vertical and lateral direction such that the corresponding difference signals (see Fig. 2.9) are  $\sim 0$ .

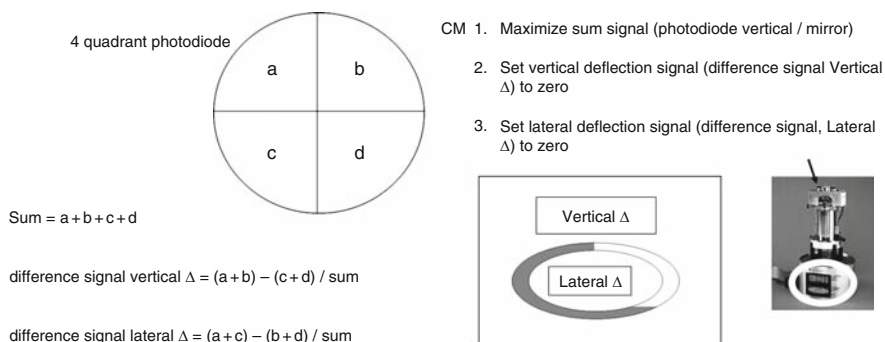


**Fig. 2.9** Schematic of photodetector and differential output signals. The top LCD display shows the vertical deflection signal and the lower panel the lateral signal, while the sum signal is displayed as a bar in the ellipse on the lower part of the round display (see schematic)

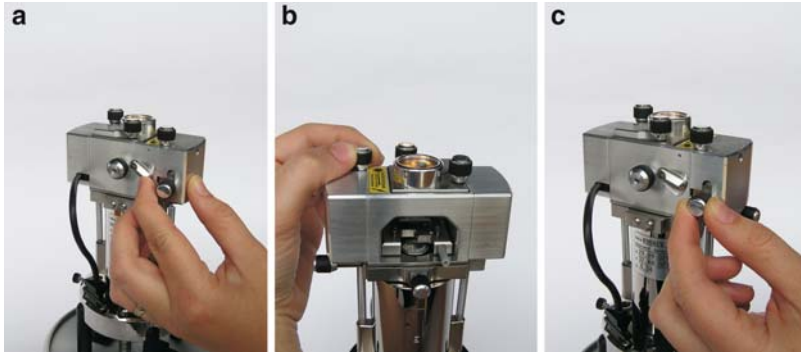


**Fig. 2.10** Adjustment of mirror and photodetector position: (a) optimizing the mirror position; adjustment of (b) vertical and (c) lateral photodiode positions

The adjustment of the mirror rotation angle and the vertical and lateral positions of the photodiode are shown in Fig. 2.10.

To prepare the set up for an experiment, the sample should be mounted. For this purpose, we remove optical head, after driving the stepper motor upward to protect the tip and the sample from unintended contact. The sample (mounted to the sample puck; see Sect. 2.2.2) is placed on the piezo scanner in center position. Finally, the optical head is placed again carefully on scanner (please ensure that the tip is far from the sample) and, *with utmost care*, is secured with the springs (for warning: see above).

The set up is now in principle ready to start an experiment. The coarse approach is carried out to position the tip close to (but not in contact with) the sample surface. Using an eyepiece, the cantilever can be viewed from the side (or alternatively one can use a top-view CCD camera for this purpose). With the eyepiece, we locate the reflection of the laser light on the cantilever and its reflection (mirror image) on the sample (red spots). Using the stepper motor, we lower the optical head until the spots are close; however, we still want to clearly be able to detect a gap between the spots. In older scanner types, the optical head is lowered by using the stepper motor for one pod of a tripod, while the other two are lowered manually using the corresponding screws. In this case, it is essential that the head is lowered such that it stays leveled at all times.

With a top-view CCD camera, we bring the camera in focus on the cantilever and then on the sample surface. Subsequently, we move the focal plane upward. Using the stepper motor, we lower the optical head until cantilever becomes sharp in focus. Following both approaches, the tip is now  $< \text{several } 100 \mu\text{m}$  away from the surface.

The fine approach for CM is carried out by the controller in an automated fashion. Before this approach and the start of the experiment are explained, the photodiode position must be adjusted. The position of the photodiode is changed such that the lateral deflection signal is set to 0.0 V and the vertical difference signal is offset to  $-2.0$  V. The vertical deflection setpoint is entered as 0.0 V in the computer menu. Upon contact with the surface as a consequence of a lowered

optical head, the cantilever will bend upward (resulting in a more positive photodiode signal). By choosing the offset of  $-2.0$  V, we limit the descent of the head and the tip to the vertical deflection setpoint of  $0.0$  V (i.e., upon lowering the tip, the controller will start scanning with active feedback loop control once the deflection signal reads  $0.0$  V).

Before the scan is started, the sensitivity of the feedback loop is adjusted by a default setting of the gains: integral gain:  $2.0$ ; proportional gain:  $2.0$ ; differential gain:  $0.0$ . The tip and sample are protected against damage by opting for a small initial scan size (e.g.,  $1\ \mu\text{m}$ ) and a low scan rate ( $3.0$  Hz). If all these parameters have been adjusted and the vertical deflection signals have been checked, we can start the scan by pressing the “engage” button.

During the descent of the tip, we closely monitor both vertical and lateral deflection signals on the LCD panels. Some variation of these signals (flickering) due to interference effects is typically observed. Upon descent, the vertical deflection signal may change monotonically, in particular for soft cantilevers for decreasing tip–sample separation distances close to physical contact. This cantilever deflection is caused by long-range forces, such as electrostatic forces, between surface and tip. By contrast, the lateral signal should *not* change monotonically. Unless tip and sample (or some protruding parts of the cantilever holder and the sample) are in contact, the lateral signal can only show the mentioned variations. If the lateral deflection signal changes its value monotonically, the engagement procedure must be stopped immediately and the tip/cantilever assembly and sample roughness must be checked to prevent unwanted contact.

The stepper motor of the AFM will reduce the tip–sample separation distance until the actual value of the vertical deflection and the chosen setpoint ( $0.00$  V) coincide. Once the values are equal, the descent stops and the scan starts automatically according to the preset parameters.

Successful tip engagement on the surface is characterized by a jump of the vertical deflection signal from some negative value to  $0.00$  V differential signal. The force with which the tip engages depends on the magnitude of the jump. If the jump is not noticeable, the upward deflection of the lever as a result of long-range forces may have been such that the differential signal reached  $0.00$  V without the tip reaching physical contact with the surface. This situation is called, “false engagement.” It can be faithfully identified by choosing a higher setpoint value for the feedback loop, e.g.,  $+1.00$  V, which corresponds to higher imaging forces. Only if the surface is within reach of the  $z$  travel of the piezo scanner, will an image be obtained, the difference signal show a value equal to the setpoint value, and the scanner’s  $z$  center position (indicated on the AFM image panel) stay within the max/min limits. If the  $z$  center position goes out of limits, the piezo is fully extended; however, it cannot reach the setpoint value. Thus, no physical contact between tip and sample had been established. In this case, the tip is withdrawn *once* from the surface (using the appropriate software command), the vertical deflection value is set again to  $-2.00$  V, and the engagement procedure is started again. Depending on the tip–sample forces and the cantilever spring constant, this procedure needs to be repeated several times.

After successful engagement, the gains must be adjusted and the imaging force (i.e., the setpoint) should be minimized. The adjustment of the gains, which regulate the sensitivity of the feedback loop and thus the accuracy with which the controller maintains the constant force value, is best done by analyzing the height and deflection signals in the so-called scope mode. The scope trace and retrace correspond to the currently captured signals for one scan line (back and forth). By increasing the gains in small increments, we aim at a minimized error (i.e., deflection) signal as we operate the AFM in constant force mode. Too low gains result in inadequately maintained setpoint value, i.e., imaging force, and thus a “height” image that does not represent topography of the scanned sample. In fact, at very low gains, the cantilever bends when the tip encounters high features and the image conditions represent “constant height” conditions. In this case, the deflection signal shows pronounced contrast (Fig. 2.11a). For increased gains (Fig. 2.11b), the height image displays the expected profile, however, the residual deflection at the edges shows that the force is by no means kept constant. With appropriate gains, the deflection contrast is vanishing, except for locations with steep changes in topography, while the height image (that displays the  $z$ -travel of the piezo required to maintain a constant setpoint force) shows an adequate profile (Fig. 2.11c). If the gains are set too high, the piezo scanner will show clearly discernible uncontrolled feedback (overdrive) seen as overshoot at steep topographic features or even oscillations (Fig. 2.11d, e). Depending on the magnitude and frequency, this unwanted feedback can be audible.

The gains do require adjustment if we alter the scan rate, the scan size, and the setpoint, i.e., the imaging force. It is particularly important to remember that both scan size and rate influence the tip velocity, i.e., if the scan size is increased, the rates should be decreased correspondingly if the feedback loop should operate with a similarly negligible error. Thus, the force and parameter settings that were optimized for a scan size of  $1 \times 1 \mu\text{m}^2$ , cannot be the same for a scan size of  $10 \times 10 \mu\text{m}^2$  at constant scan rate, as the tip velocity is increased by a factor of 10.

The appropriate force setting is performed in the force–distance mode (Fig. 2.12; for details see also Sect. 4.1 in Chap. 4). In this mode, the deflection of the cantilever is monitored as a function of sample/piezo position, while the tip is brought periodically in and out of contact with the sample surface. The measured cantilever deflection  $z$  can be converted to the corresponding force  $F$ , by applying Hooke’s law, if the spring constant of the lever  $k$  is known ( $F = k \Delta z$ ).

The adhesion between tip and sample is characterized by the so-called pull-off or pullout force, which corresponds to the jump in deflection (force) in position 5 in Fig. 2.12. When performing an AFM scan, this force will pull tip and surface together. In addition, the tip may apply an extra force (load) on the surface, depending on the preset value of the setpoint force. The imaging force is the sum of this load and the contribution of adhesion (Fig. 2.13). By reducing the load, the imaging force is reduced as well. However, the pull-off force represents a limit below which stable imaging is not feasible. One may work against the adhesion by selecting a negative load; however, once the tip pulls off the surface, the feedback loop will cause a full retraction of the piezo as the setpoint value is smaller than the

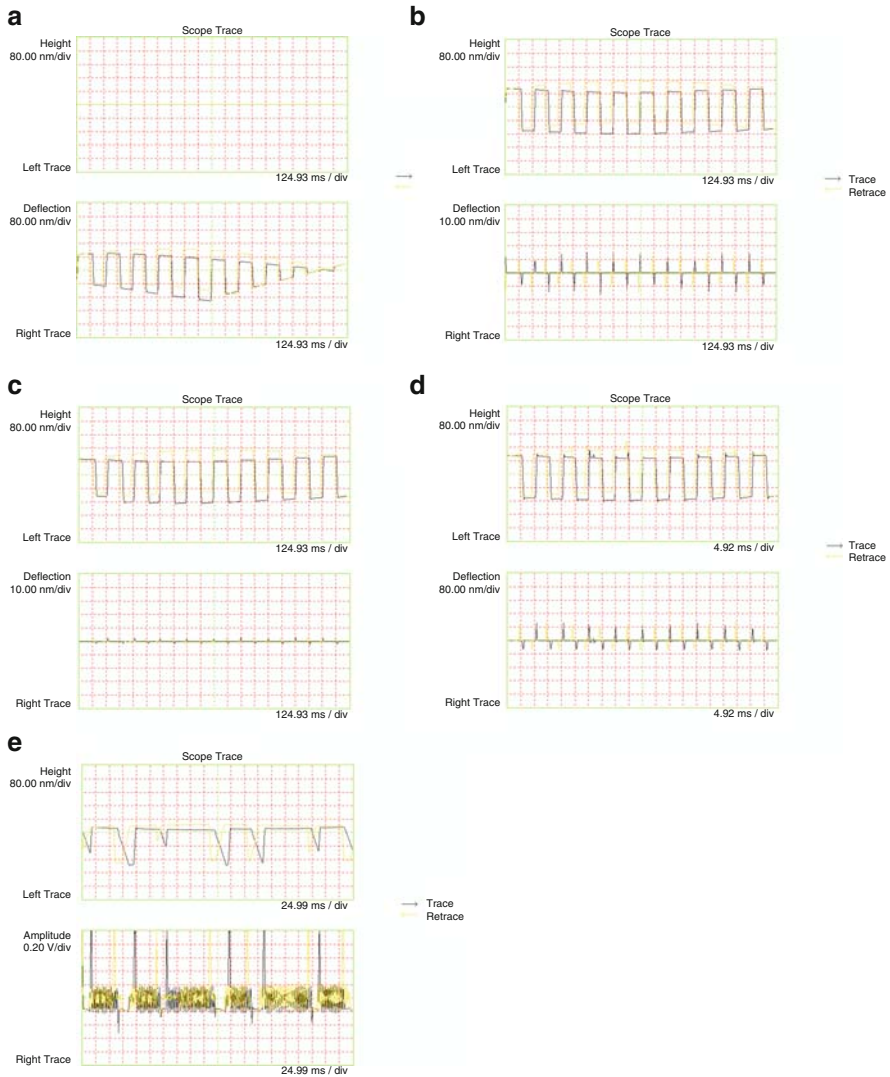


**Fig. 2.11** Scope traces for TM-AFM height and amplitude images recorded for different gain settings (details see text)

actual deflection signal (which corresponds to the signal of the now freely suspended lever). In addition, the magnitude of the adhesive forces depends on the radius of the particular tip used (Sect. 4.1 in Chap. 4).

The magnitude of the pull-off force also depends on the imaging medium as intermolecular forces may depend on the medium (Chap. 1) and since in ambient conditions water may condense at the tip–surface contact, giving rise to the well-known capillary forces. Thus, by performing experiments in liquid media, such as

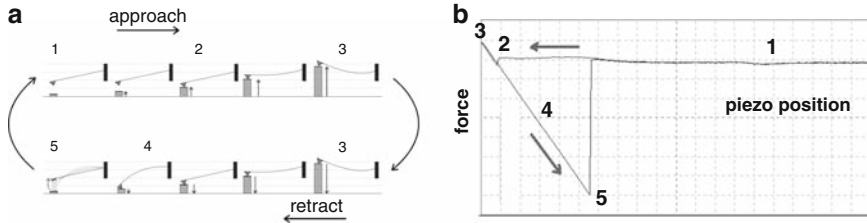


**Fig. 2.12** (a) Measurement of force–distance curves (schematic representation). The sample is approaching the tip (1); at some distance the gradient of the force overcomes the cantilever spring constant and the tip jumps into contact (2); further movement up causes a deflection of the cantilever (3), during the retraction the tip sticks usually much longer (4) and snaps off, when the spring constant overcomes the force gradient (5). (b) Corresponding output: force–displacement plot. Reproduced with permission from [1]

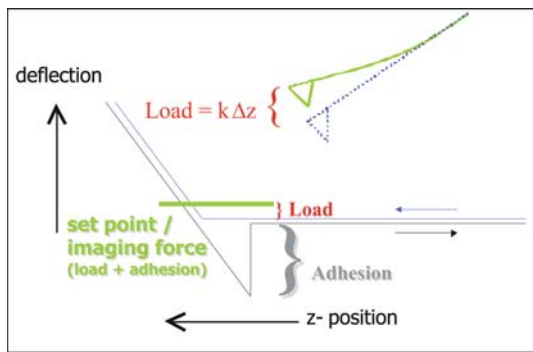


**Fig. 2.13** Schematic of force displacement curve and relation of load, adhesion (pull-off force), and imaging force on the one hand and setpoint on the other hand

water, or in dried gas atmosphere, the often overwhelming contribution of capillary forces can be avoided or reduced.

Once all imaging parameters are set, data can be acquired and captured. It is important to note that the data may depend on the actual settings (force, scan velocity, feedback loop quality, etc.); therefore, one should note these parameters independently. The data displayed on the screen is typically plane-fitted to be readable (in case the sample plane does not coincide with the horizontal  $x, y = 0, 0$  plane of the scanner, the image would appear tilted and flat surfaces would appear in saturated colors; compare also Sect. 2.2.7). A line-by-line plane-fit is most often utilized. Here, the data of each captured scan line is normalized by subtracting a first order polynomial fit from the particular line. The captured data, however, should be captured without plane-fit in order to facilitate meaningful analysis at a later stage (Sect. 2.2.7).

A final remark refers to the  $z$  center position of the scanner. Because of thermal and other expansions, e.g., as a result of temperature equilibration, especially on

rougher samples, the  $z$  center may go out of limits. For samples with excessive roughness or pronounced sample tilt, this may occur, depending on lateral scan size, right after engaging the tip.  $Z$  center out of limits means, as alluded to above, that the scanner/feedback loop cannot reach the setpoint value. In case of a fully extended scanner, this is of no consequence other than the absence of AFM data; however, in the situation of a fully retracted piezo, the tip must be immediately withdrawn to avoid sample and probe damage.

### 2.1.2 Stand Alone AFM (Contact Mode)

The steps for setting up a stand alone (tip scanning) AFM are very similar to those for CM. Again, each AFM brand has its own peculiarities, but the general features are very similar. In Fig. 2.14, the entire set up of a stand alone microscope, including transparent environmental chamber, is shown. In the following pages we quickly summarize the basic steps of assembly, keeping in mind that the conceptual differences to the previous paragraphs are minor.

The individual parts are shown in more detail in Fig. 2.15.

Mounting the cantilever to the scanner requires (in addition to the scanner, the cantilever, and tweezers) a special tool to release the force of the clamping mechanism (clip, compare Fig. 2.16a). The tool lifts up the clip as shown below in

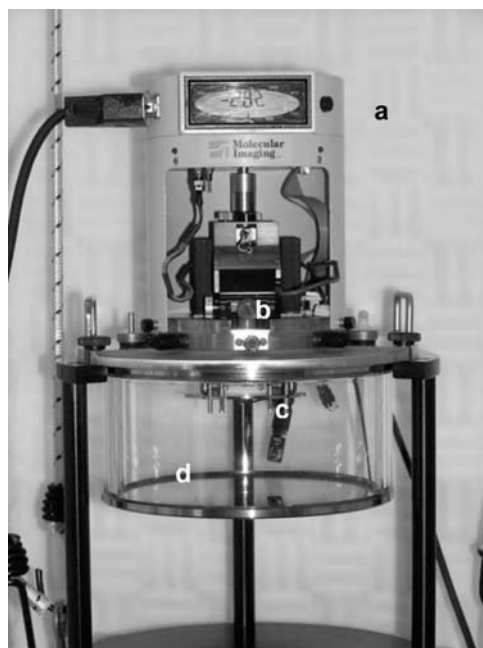


**Fig. 2.14** Fully assembled stand alone AFM comprising (a) the base (incl. LCD display), (b) scanner and photodetector, (c) sample, and (d) environmental chamber

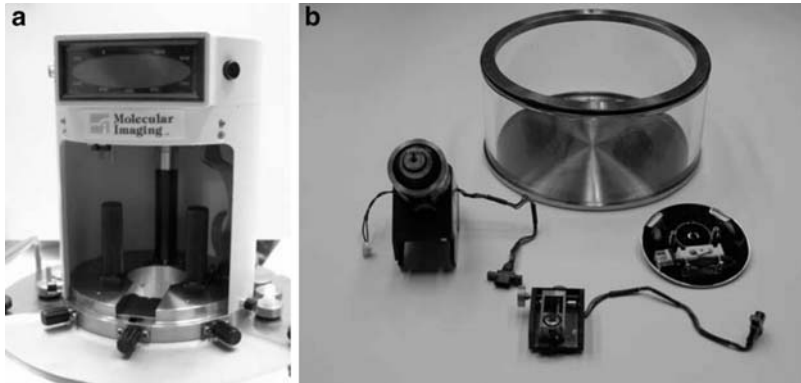


**Fig. 2.15** (a) AFM base and (b) scanner, photodetector, sample mount (*front left to right*), and environmental chamber (*back*)

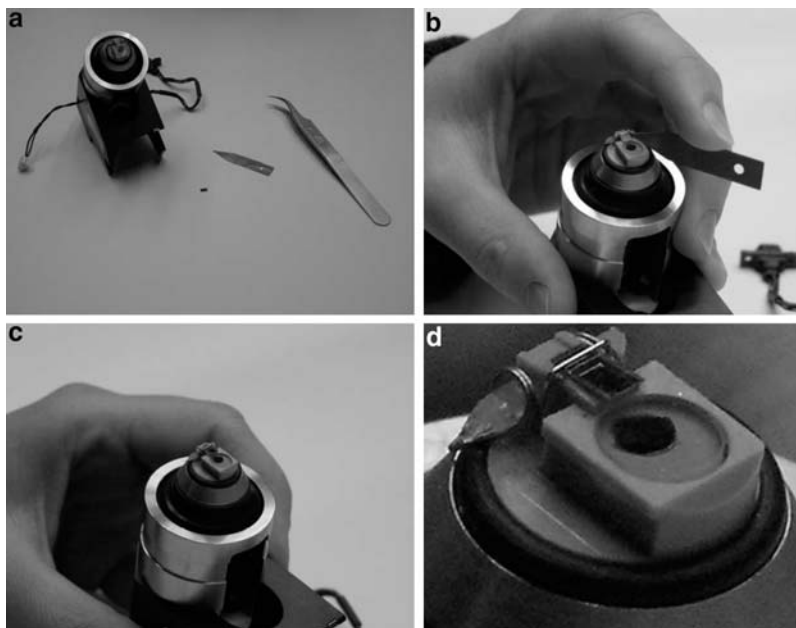


**Fig. 2.16** Insertion of probe as described in the text

**Fig. 2.16b.** The cantilever chip can be inserted gently under the lifted clip, aligned with the shape of the holder, followed by releasing the clip.

First, the scanner (incl. the previously mounted cantilever/tip) is inserted upside down into the base (Fig. 2.17). Subsequently, the scanner cable is attached.

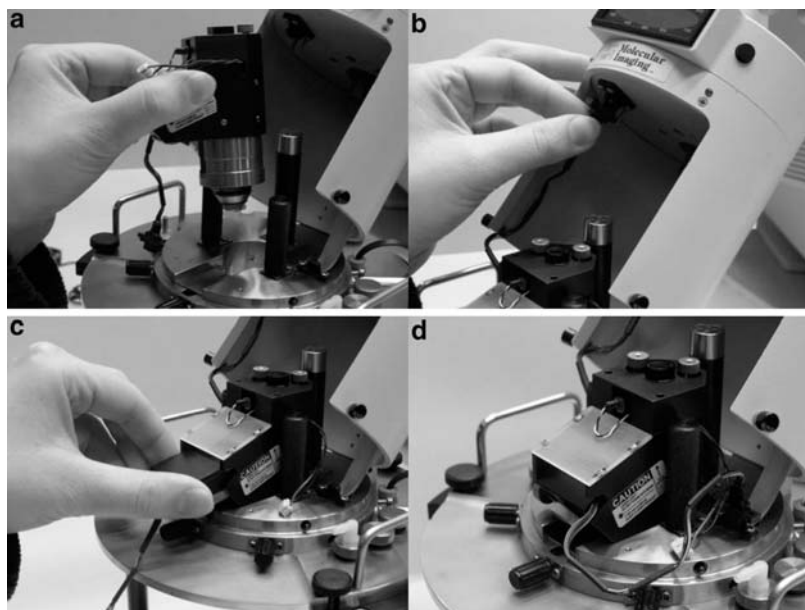


**Fig. 2.17** (a, b) Mounting of scanner; (c, d) attachment of photodiode



**Fig. 2.18** Mounting of sample

The separate photodetector is mounted subsequently as depicted in panel (c) in the scanner side port and connected to the base through the cable.

The sample is immobilized on a metallic sample puck (see arrow) on the sample holder plate (Fig. 2.18a). This plate is finally attached from below as shown by several screws. Care has to be taken not to touch the probe tip as a result of inadequate screw positions.

The laser is adjusted by turning the corresponding screws on the laser stage (Fig. 2.19), similar to the procedures described for the scanning sample AFM. The laser alignment can be checked by visual inspection of the laser light as it is reflected on a sheet of paper below the base. Panel (b) shows the situation in which laser light does not reflect off the cantilever (round spot), while in panel (c) a typical reflected spot can be recognized. In addition to the paper, the reflected light is seen on the

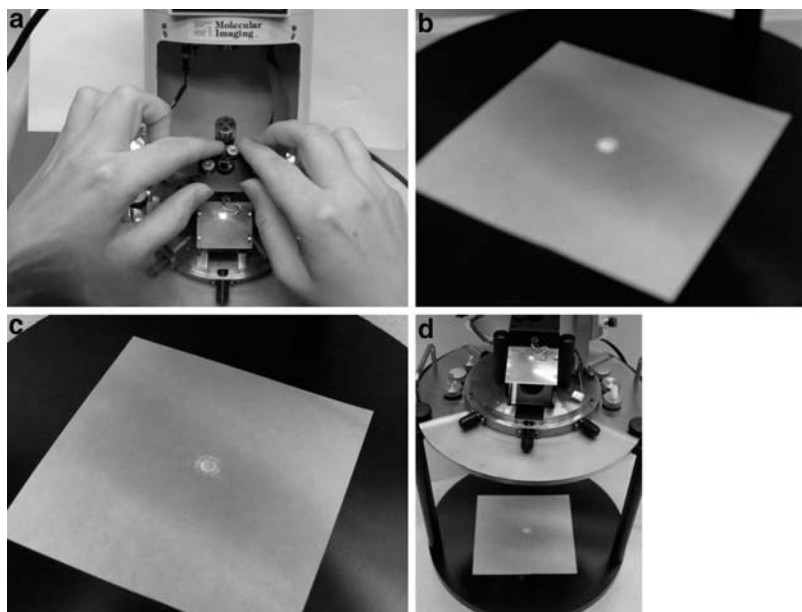


**Fig. 2.19** Laser alignment: (a) Adjustment of laser stage by laser stage screws; (b) laser light reflected off a piece of paper for off cantilever position; (c) same for on cantilever position; (d) in addition, the spot can be analyzed on the reflection on the scanner window

scanner (Fig. 2.19) window (panel d). If the laser light reflected off the cantilever reached the photodiode, a maximized signal is indicative of an appropriate alignment. The differential deflection signal is read as an Arabic number directly from the LCD display, as shown in Fig. 2.14, while the sum signal is displayed in the ellipse on the lower part of the display. The display can be switched to the lateral deflection signal by using a small switch (Fig. 2.19).

The protocol and settings for the engagement process and the imaging are essentially identical to the procedures discussed earlier and we refer here only to this section and the corresponding manuals (if applicable).

### 2.1.3 Intermittent Contact (Tapping) Mode

The prime differences among the different AFM modes, such as CM (discussed above) and intermittent CM, as elucidated in the following section, are the feedback parameters and the choice of the cantilever. For intermittent contact (tapping) mode AFM, a stiff cantilever ( $k$  typically 10–50 N/m) with a resonance frequency of 100–400 kHz is chosen. The cantilever, which is inserted in an identical manner as for CM into the cantilever holder, is excited to vibrate by an integrated piezo actuator. Instead of deflection (contact force), the amplitude of the forced oscillating lever is detected, analyzed, and utilized in the feedback loop (Fig. 2.20).

- TM 1. Maximize sum signal (photodiode vertical / mirror)
2. Set vertical deflection signal (difference signal Vertical  $\Delta$ ) to zero ! *Other position !*

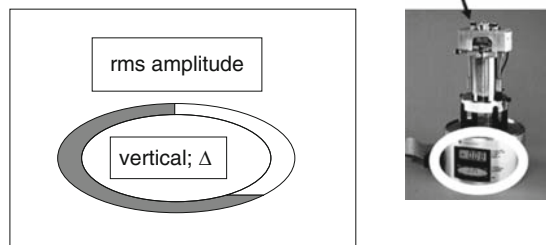


**Fig. 2.20** Schematic of adjustment of photodiode signals for TM. Note that the LCD display shows a different signal compared to contact mode

Practically speaking, the laser alignment is performed for CM; then the base is switched with a toggle switch (DI multimode) to tapping mode. This changes the LCD display information.

A first difference compared to the details of CM operation is noticed when the cantilever has been inserted and the laser positioned such that the reflected light is centered on the photodetector: one has to locate the resonance frequency and set an appropriate excitation frequency. This procedure is called cantilever tuning. We strongly suggest not to use the built-in automated routine, but to perform this simple operation manually.

For this purpose, the cantilever tune menu is opened and a frequency sweep is performed. From the probe manufacturers data sheet, the resonance frequency is approximately known, e.g., 300 kHz. Hence, we excite the lever with low power (drive amplitude 25 mV) and sweep the frequency for  $\pm 30$  kHz around the expected resonance frequency of 300 kHz. In advanced AFM set-ups, the resonance frequency may also be independently determined before the tuning by a thermal tune (please consult the corresponding manual for details; the procedure is globally reviewed in Sect. 2.2.5).

The amplitude of the cantilever should display a maximum at the resonance frequency  $f_{\max}$ . If this is not found, the sweep width (in case the resonance frequency lies outside the scanned range) and subsequently drive amplitude may be increased (in case the amplitude is too small to be detected) (Fig. 2.21).

After the resonance frequency has been localized, we set the operation frequency to  $f_{\max}$  or to the frequency at which the amplitude is  $\sim 85\%$  of the maximum amplitude  $A_{\max}$ . This latter choice has been shown to be beneficial to reduce the imaging forces. Subsequently, the phase signal is zeroed (the phase lag between excitation vibration and cantilever reaction is set to zero) and finally the amplitude is

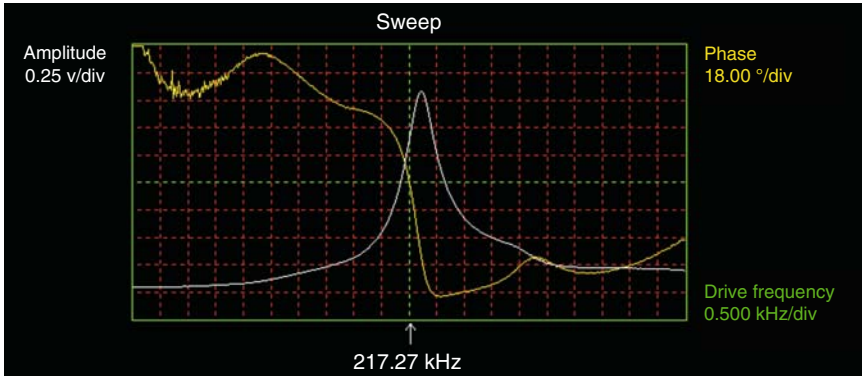


**Fig. 2.21** Amplitude  $A$  (curve with maximum) and phase response of TM–AFM cantilever

adjusted. This can be done by setting a particular drive amplitude in order to reach a chosen (cantilever) amplitude. The exact value of the amplitude is chosen depending on the nature of the sample (for details: see the corresponding hands-on example). As a rule of thumb, we can state that the cantilever amplitude should be as low as possible to ensure smallest possible peak forces; for glassy samples imaged in ambient air, it can be as low as 25 nm (DI multimode: ca. 0.5 V), while for viscoelastic samples and polymers, above  $T_g$  higher amplitudes (up to 200 nm; 4.0 V) may be required to overcome tip–sample adhesion. During the experiments, the appearance of the images and the constant small value of the deflection signal are good indicators for appropriate tapping. If the amplitude is too small, the tip cannot overcome the attractive interactions and remains pinned on the surfaces, while the sample is being scanned. Hence, the stiff probe is dragged over the surface, resulting in (1) sample damage and (2) useless AFM data.

Occasionally the resonance peak looks unsymmetric or distorted; it is also possible that multiple peaks are observed in the frequency scan. These ill-shaped peaks are either the result of an ill-behaved resonance due to misfabrication of the lever; however, often the coupling of the excitation vibration of the incorporated piezo oscillator and the cantilever chip are responsible. The reader is encouraged to remove the cantilever holder and subsequently the cantilever chip from the holder; the cantilever is then placed again into the holder and secured with the corresponding clip. If this change in position and clamping in the holder does not help, the reason for the unsymmetric resonance may be indeed the particular cantilever. As long as the resonance peak can be identified and the slope of the resonance peak is steep enough, the lever may still be used for imaging.

Before the AFM experiment is started, the scan parameters must be adjusted. First of all the tapping AFM menu must be chosen; compared to CM, there are a number of changes: the scan rate must be reduced (max. 1.0 Hz) and the gains are typically set to lower values (integral gain: 0.5; proportional gain: 1.0; differential gain: 0.0).

The manual tip–sample approach should be carried out with extra care to avoid unintentional tip–sample contact. Most tapping mode levers are made of silicon, which is brittle. Therefore, tip–sample contacts may easily lead to tip damage.

The engagement procedure is simplified compared to CM since the stiff tapping mode levers do not bend as a result of long-range forces. However, it is still advisable to monitor the amplitude signal on the LCD display. The actual setpoint value is determined (during the preengage check) and preset by the AFM controller (using a particular software routine). If the amplitude happens to drop to zero before the surface has been reached, the descent must be aborted. Likely, there has been contact between the sample and the tip/cantilever/holder resulting in the complete damping of the forced oscillation.

False engagement is also possible in tapping mode and can be attributed to damping of the cantilever vibration by the air cushion in between tip and sample. Similar to CM, there is a simple check whether the probe is really engaged: The setpoint is *lowered* slightly (corresponding to *increased* amplitude damping and hence *increased* forces). *Please be aware that the sign of the change is opposite to contact mode!* If the surface is within reach of the  $z$ -travel of the piezo, an image will be displayed and the amplitude display will show the setpoint value (rms voltage). In addition, the scanner's  $z$  center position will show a value between max/min. In case of false engagement, detected by a  $z$  center position out of limits and an rms amplitude value unequal to the setpoint, we withdraw the tip once and restart the engagement procedure.

After successful engagement, the gains must be adjusted and the imaging force should be minimized (i.e., the setpoint maximized, see above). The adjustment of the gains is performed best in the scope mode. By increasing the gains in small increments, we aim at a minimized error (i.e., amplitude) signal since we operate the AFM in constant amplitude mode. If the gains are set too high, the piezo scanner will show clearly discernible uncontrolled feedback seen as oscillations. These are first recognized in the amplitude and phase images.

It is not advisable to adjust the amplitude setpoint settings in the amplitude–distance mode (Fig. 2.22). Here, a too high damping that would be present when the

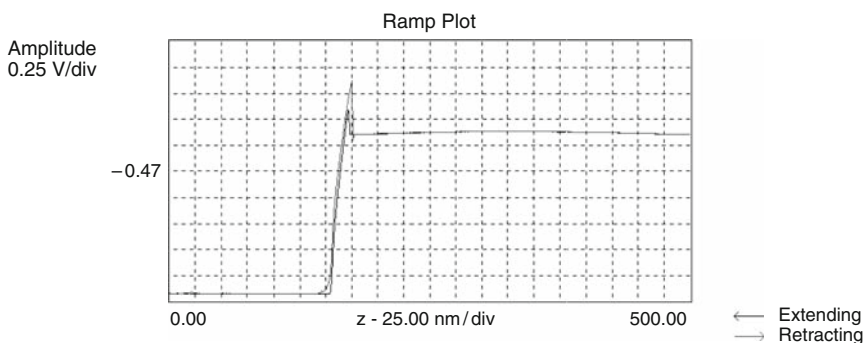


**Fig. 2.22** Typical tapping mode amplitude–distance curve

entire curve is recorded, as shown in the figure, may result in tip damage. In this mode, the amplitude of the cantilever is monitored as a function of sample/piezo position, while the tip is brought periodically in and out of contact with the sample surface.

Instead, it is advisable to follow an alternative strategy. We will first determine the rms amplitude of the freely forced oscillating lever. This is done by selecting a setpoint higher than the amplitude adjusted during tuning. This setpoint value cannot be reached by the AFM controller/set-up; the feedback loop will retract the sample in order to minimize the damping; yet even after full retraction to its minimum length, the actual rms amplitude is still below the chosen setpoint value. However, the value is displayed on the LCD display and can be noted. As a setpoint for imaging, we may now choose a value that corresponds to 90%, or less, of that value. Setpoint ratios of  $\sim 0.90$ ,  $\sim 0.75$ , and  $\sim 0.4$  have been attributed to soft, intermediate, and hard tapping conditions, respectively by Magonov et al. [2].

## 2.2 Practical Issues of AFM Operation

### 2.2.1 AFM Cantilevers, Tips, and Their Characteristics

For different modes and purposes, there are special AFM probes (cantilevers and tips). These differ in terms of their geometry, dimensions, force constants, resonance frequencies, tip position, shape and radius, material, etc. There are numerous commercial sources and we refer to these for finding the appropriate probes for the given experiment and sample. It is also clear based on the rudimentary treatment of tip-sample interactions (Chap. 1) and the basic AFM features that the attainable information and resolution are in many cases dictated by the properties and characteristics of the probe tip. The tip physically interacts with the surface and its sharpness and aspect ratio, for instance, determine the degree of convolution in imaging small features or the limited success in the visualization of small pores (Fig. 2.23).

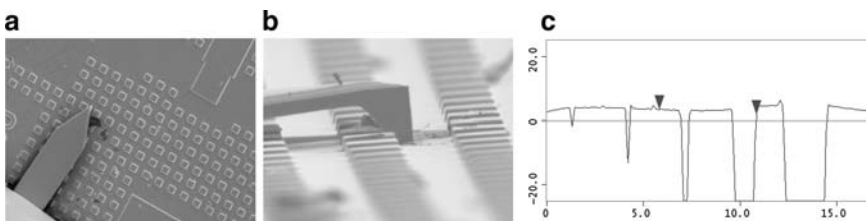


**Fig. 2.23** (a) Top-view and (b) side-view SEM image of probe tip in contact with a patterned elastomer sample. (c) Section of an AFM micrograph of micro- and nanopores of identical depth fabricated in silicon showing the limited ability of the tip to penetrate into the pores

AFM cantilevers and tips can be differentiated based on some central characteristics that are summarized below.

|   |  |
|---|--|
| <i>Material</i>                         | <i>Geometry</i>                                    |
| Silicon                                 | Single beam cantilever                             |
| Silicon nitride                         | V-shaped cantilever                                |
| Metal or diamond coated levers and tips | Tip shape: pyramidal (opening angle, aspect ratio) |
| Diamond tips                            | Inclination angle of tip                           |
| Chemically functionalized probe tips    | Tip position on cantilever                         |
| etc.                                    | Oxide sharpened                                    |
| <i>Special properties</i>               | etc  |
| Conducting                              | <i>Relevant physical parameters</i>                |
| Actuated                                | Length   |
| Thermal sensor equipped                 | Width  |
| Chemically distinct coating             | Thickness  |
| etc.                                    | Spring constants                                   |
|   | Resonance frequency                                |
|   | Tip radius   |
|   | etc  |

### 2.2.1.1 Contact Mode Cantilevers and Tips

Electron micrographs of typical levers and tips are shown below to illustrate some representative examples and dimensions (Fig. 2.24).

Because of misalignment in the production process, the tip may not always be situated symmetrically on the long cantilever axis. This type of error in tip position may lead to erroneous readings of deflection as vertical and torsional deflections are coupled (Fig. 2.25).

Intermittent contact (tapping) mode probes are depicted in Fig. 2.26, while special AFM probes are shown in Fig. 2.27.

### 2.2.2 Sample Preparation

One notable difference of AFM in comparison with electron microscopy is the ease of sample preparation. There is no need for conductive coatings, thin sections, etc. This means that any polymer sample can in principle be analyzed by AFM, provided the part fits into the corresponding microscope. There are also stand alone AFM models that can operate on any large macroscopic surface, such as an airplane wing, to perform local analysis.

However, since AFM measures topographic and other information using a sharp tip with typical dimensions of several micrometers, opening angles of  $<20^\circ$  to  $>35^\circ$ , and radius of curvature of 5–50 nm (or larger), sample roughness is a crucial issue. This is also true because of the limited  $z$ -travel of most common piezo transducers, which limits the difference between the highest and lowest point on the scanned

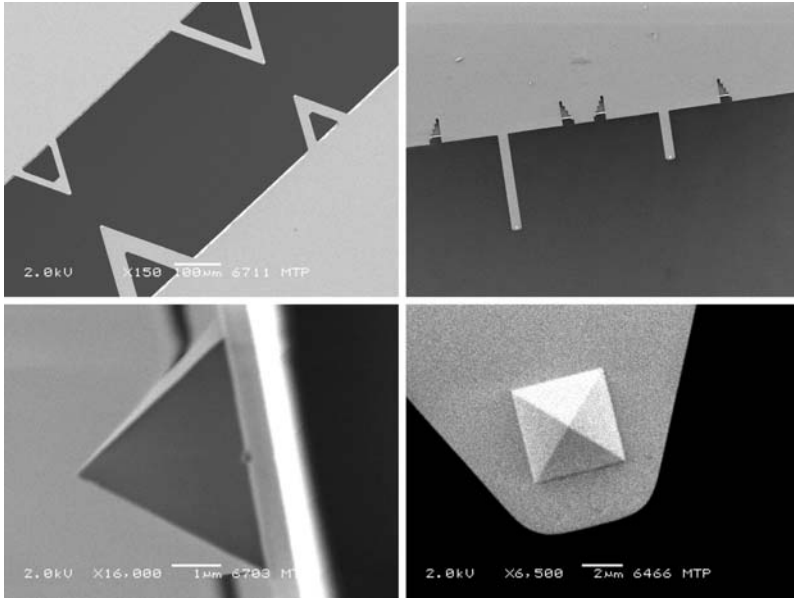


**Fig. 2.24** SEM images of CM cantilever (V-shaped and single beam) and microfabricated tips

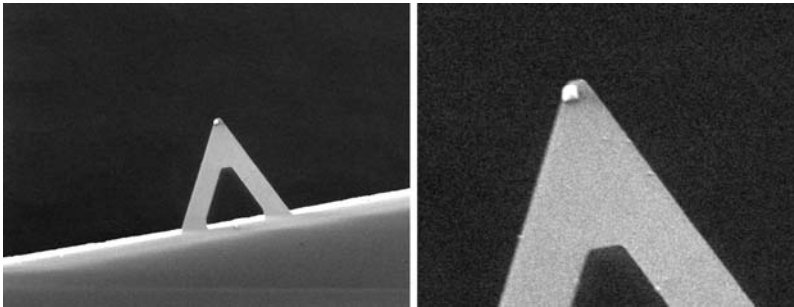


**Fig. 2.25** SEM image and digital zoom of misfabricated CM cantilever: the microfabricated tip is located off the central axis of the lever

surface to several micrometers. Pronounced roughness in excess of the  $z$ -travel or in conflict with the physical shape of the probe may result in heavily convoluted images (see e.g., Figs. 2.42 and 2.43). Therefore, sample preparation should provide smooth sample surfaces with low roughness.

For polymers, we can differentiate different sample preparation procedures that aim at providing smooth films or surfaces or at exposing the interior of bulk samples at a specimen surface.

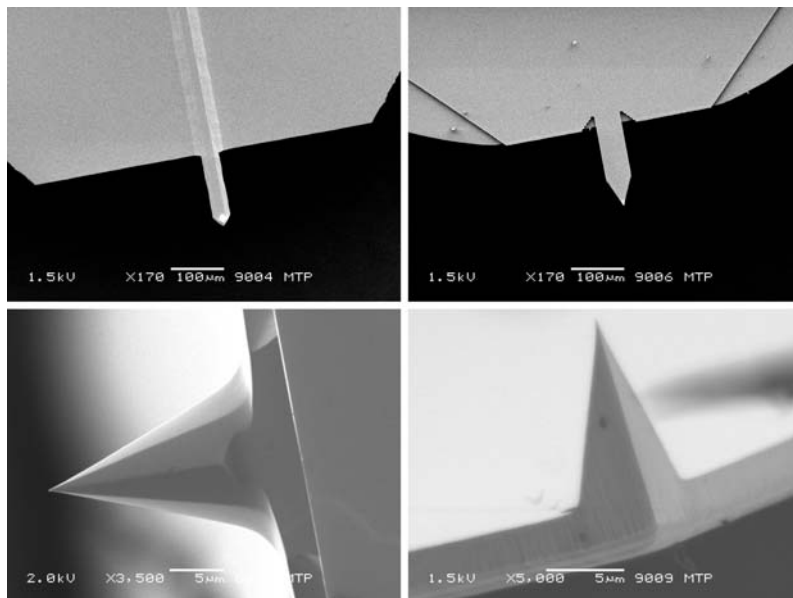


**Fig. 2.26** SEM images of different TM cantilevers and microfabricated tips

In solvent casting, a thin film is prepared on a solid substrate by casting a solution of polymer onto the substrate, followed by evaporation of the solvent. Thicker films with some control over film thickness can be prepared. Enhanced control over thickness is achieved in the so-called doctor-blading approach, where the thickness of a viscous polymer solution is adjusted down to the 10 nm range by removing excess solution using a knife (the knife–substrate spacing is controlled).

Spin-coating exploits centrifugal forces and rapid evaporation of the solvent to prepare films with controlled thickness and roughness. Here, a polymer solution is deposited on a cleaned substrate, which is spun with high velocity around its central axis. The solution spreads and is spun off the substrate, leaving a film behind. The thickness can be controlled by the polymer concentration ( $d_{\text{film}} \propto \text{conc.}$ ) and the rpm ( $d_{\text{film}} \propto \sqrt{\text{rpm}}$ ).

The interior of bulk samples can be revealed by fracture, freeze fracture, or (cryo-/ultra)microtoming. These techniques are well established in electron microscopy and require substantial training to ensure that the knives used do not introduce scratches and other artefacts. Unlike in SEM or TEM analysis, however, it is very well possible to analyze the trimmed specimen instead of the very thin sections removed (cryofacing). This loosens the constraint of ultrathin sections in many applications. Care has to be taken that the sample to be imaged is not significantly thicker or thinner than the calibration grating used for scanner calibration (see Sect. 2.2.5)

Crucial for all AFM experiments, independent of the sample preparation method and also in the absence of any sample preparation, is the firm attachment of the

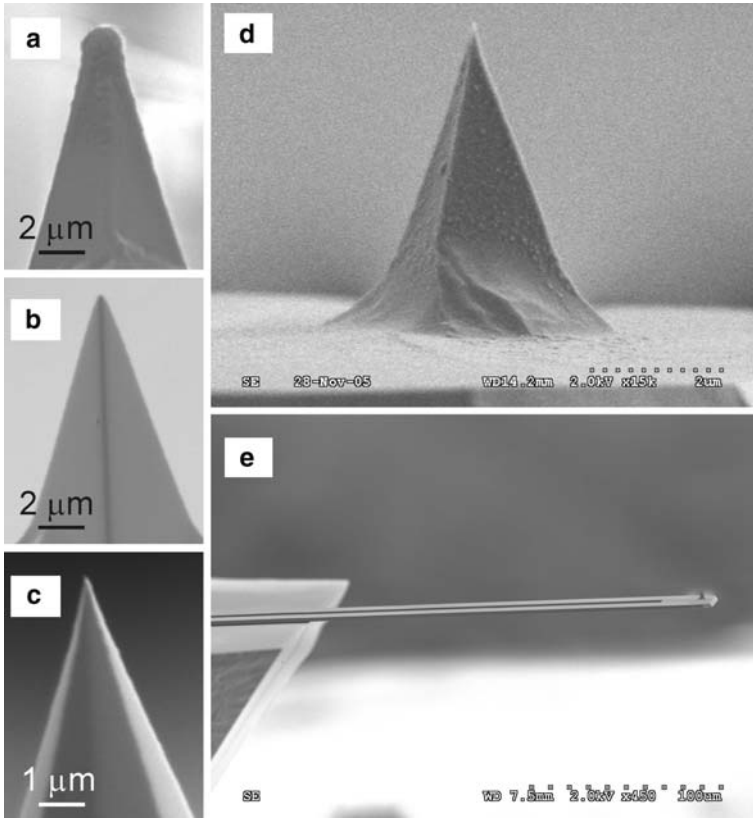


**Fig. 2.27** SEM images of different specialized AFM probes: (1) tips of widely different radii (a) 870 nm, (b) 150 nm and (c) 20 nm; (d, e) thermal probe and tip (images courtesy Anasys Instrument Inc.)

corresponding samples to the AFM sample holder. Many AFM types rely on ferromagnetic metallic pucks that are attached to a strong magnet on the scanner.

Samples in the form of freestanding polymer films, sections, microtomed specimens, or substrate-supported sample must be *firmly* attached to the sample pucks. In some cases, samples may be deposited straight onto the pucks, such as for instance polymer colloids. A second requirement for attachment is that the sample specimen's surface is exposed in a flat and leveled fashion in order to reduce possible shortcomings of the scanner maximum z travel.

Double-sided sticky tapes are popular for the attachment of samples. Various brands and types are available. For many routine measurements conventional tape is sufficient; however, some thicker variants may lead to problems when pressure is exerted to fix the samples, since the tape will relax and hence cause substantial drift in the AFM image. A similar effect may be present as a result of thermal expansion, when a "cold" AFM is operated with high resolution in the first hour(s)

of operation. Among the many parts that may contribute to the drift, the sticky tape is one. Particular problems with tape have been observed for measurements in liquid media (compare Sect. 3.3).

Alternatively, different types of glue, including epoxy or cyanoacrylate-based glues, can be used. Care has to be taken to avoid sample contamination. In particular, cyanoacrylates must not be covered during curing as they outgas material that deposits on the sample if covered.

### **2.2.3 Choice of Operation Modes and Suitable Imaging Environments**

The choice of operation modes and, if applicable, suitable imaging environments depend on many factors, including the type of polymer system to be analyzed and the type of information that is required. Biologically relevant materials or effects that are intrinsic to the liquid–solid interface, for instance, require, of course, AFM under liquid. For a number of experiments, these almost trivial considerations dictate the choice and we refer to the hands-on sections in the corresponding chapters for more detailed information.

#### **2.2.3.1 Contact Versus Tapping Mode**

One central concern with routine AFM on polymers is the presence of shear forces that occur in CM. These forces are a result of friction between AFM probe tip and the polymer sample and may deform and plastically modify the polymer surface. This has been observed even for glassy materials, such as PS, when imaged at ambient conditions (see Sect. 3.2.3 in Chap. 3; Fig. 3.16). In addition to sample damage, the tip may be affected by adhering particulates or, even worse, by wear. These phenomena limit the resolution dramatically and may result in unwanted artefacts (excessive tip imaging). Thus, minimized imaging forces are essential, and this may require the operation under a suitable liquid to eliminate capillary forces.

For many fragile materials and research/practical questions, intermittent CM is preferred as the lateral forces are practically avoided. Thus, sample damage or deformation is circumvented. However, despite the absence of shear forces, too high amplitudes or too low setpoint ratios may lead to damage of the sample or the tip as well.

### **2.2.4 Tip Handling and Modification Procedures**

Since the sharpness of the probe tip determines the attainable resolution in many cases, it is crucial that the AFM tips are handled with utmost care. In many laboratories, it is not practical to quantify the sharpness of all individual tips because this is a time consuming and challenging task. However, the sharpness of commercially available tips often varies even on the same wafer and among nominally identical probes.

Tips should be handled as described in Sect. 2.1.1 and any uncontrolled contact of the tip with any surface (i.e., without proper piezo/system feedback) must be avoided. After longer storage times (e.g., on poly(dimethyl siloxane)-based adhesive layers) or for certain experiments, cleaning of tips is necessary.

CO<sub>2</sub> snow cleaning, immersion in organic solvents, the use of UV–ozone or plasma cleaners, and strong oxidizing solutions have all been reported. Care must be taken that the probes do not touch any object unintentionally (e.g., while venting a plasma cleaner chamber) and that the reflective metal coating (if applicable) is not damaged. For many routine experiments, a simple solvent cleaning is sufficient. This is done by immersion of the cantilever chip with tweezers into a solution of high purity toluene followed by drying in a gentle stream of nitrogen (this must be done with proper safety clothing and under proper ventilation; please refer to standard chemistry literature for safety precautions).

Organic thin film (monolayer) coatings can be applied on oxide or metal (typically gold)-coated probe tips following recipes for self-assembled monolayer depositions that were adjusted for AFM probe technology. These probes are also commercially available and are useful to ensure known surface chemistry, to immobilize molecular species for assessing specific interactions, or to enable enhanced imaging conditions.

### 2.2.5 Calibration Issues

The AFM scanners are calibrated by imaging a grating of defined spacings (Fig. 2.28a). Closed loop systems require only an occasional check of the calibration of the capacitive sensors; open loop scanners, however, require, in particular for the  $x$ ,  $y$  calibration, a regular (monthly) check and calibration. For a typical AFM system, the deviation should not exceed 5%; otherwise a calibration is needed. Based on the images acquired on the gratings, automated calibration routines correct altered  $x$ ,  $y$ , and  $z$  sensitivities, scanner bow effect (Fig. 2.28b), etc.

The calibration of the  $z$  direction must be carried out, as already mentioned, on a calibration specimen that possesses identical height as the samples to be analyzed. For open loop tube scanners the calibration was reported to depend on the sample height [3], which is easy to see considering that the tube deforms such that a point on the sample surface travels on the surface of a sphere. Changing the radius of the sphere results for a given angular change in an altered path on the surface of the sphere, i.e., if the sample is thicker than the calibration grating for  $z$  calibration, lateral distances will be underestimated and vice versa.

A central question is often “how sharp is the tip?” Together with tip aspect ratio, opening angle, and tip inclination angle (taking into account that the cantilever is mounted under an angle), this defines in many circumstances the resolution.

Direct imaging with SEM or TEM can provide access to the required information (see Sect. 2.2.1). In addition, there are specially designed gratings that possess features, such as tips, that are sharper than the probes used. By scanning these features, one obtains convoluted AFM images (the information in the image is in parts due to the tip and its shape and size, and in parts due to the grating).

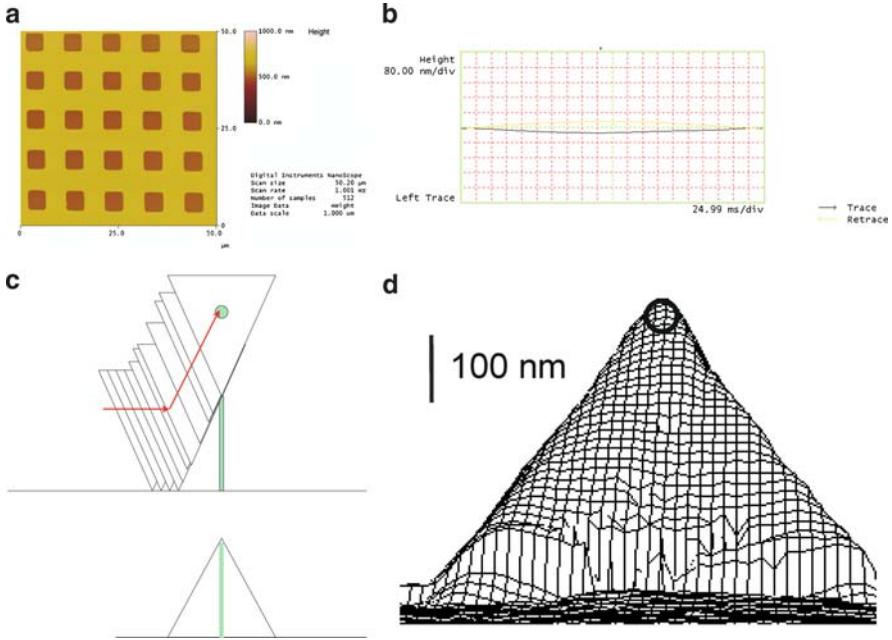


**Fig. 2.28** (a) Contact mode AFM height image of a calibration grating. (b) Cross sectional plot of an AFM height image of a flat silicon wafer displaying a pronounced scanner bow effect. This scanner must be recalibrated to correct for this bow. Any data captured should be plane-fitted accordingly (*see below*) (c) Schematic of tip imaging on a hypothetical needle (*top*); the AFM height image will display the shape of the tip itself. (d) Image obtained by contact mode AFM on a calibration grating exposing very sharp tips; the tip radius  $r$  determined was 25 nm

Similarly challenging, but nevertheless important in the context of constant experimental conditions (e.g., imaging at the same force) or force mapping, is the calibration of spring constants in CM AFM. The nominal spring constants stated by the suppliers are mere indications and cannot be trusted. This is primarily due to the impact of the cantilever thickness on  $k_N$ .

The force constants of *single beam* cantilevers (normal spring constant  $k_N$ , torsional spring constant  $k_\phi$ , and lateral spring constant  $k_L$ ) can be calculated, assuming levers of constant thickness, based on measured cantilever dimensions, from continuum elasticity mechanics of isotropic solids: [4–6]

$$k_N = \frac{Ewt^3}{4\beta^3}, \quad (2.1)$$

$$k_\phi = \frac{Gwt^3}{3l}, \quad (2.2)$$

$$k_L = \frac{k_\phi}{h^2} = \frac{Gwt^3}{3lh^2} \quad (2.3)$$

with cantilever length  $l$ , cantilever thickness  $t$ , cantilever width  $w$ , tip height  $h$ , Young's modulus  $E$ , Poisson's ratio  $\nu$ , and shear modulus  $G = E/2(1 + \nu)$ .

For Si cantilevers, the material properties (Young's modulus and Poisson's ratio) are known in any crystal orientation [7]. By contrast, the material properties of the  $\text{Si}_3\text{N}_4$  cantilevers are not well defined and may vary significantly [8] due to differences of the CVD processes [9, 10]. For instance, Young's moduli and Poisson's ratios of  $\text{Si}_3\text{N}_4$  cantilevers in the range of 120–200 GPa and 0.22–0.27, respectively, have been reported.

Procedures for the reliable calibration of normal forces (i.e.,  $k_N$ ) are well established. Several methods can be used, such as the thermal fluctuation method [11–13], the reference lever [14], or the added mass technique [15]. We will mention in the following the thermal noise and the reference lever methods in some detail.

The sensitivity of the optical deflection detection system is easily calibrated by recording an  $f$ - $d$  curve on a stiff substrate, e.g., a glass slide or a piece of silicon. The slope of the hard wall contact region in this photodetector – piezo displacement plot must be unity, as for the movement of 1 nm in  $z$  direction the tip and cantilever move upwards 1 nm as well. This function is typically implemented in the AFM software (Fig. 2.29).

Next comes the calibration of the cantilever spring constant in order to be able to relate the measured deflection to force using Hooke's law. Even though the force constants of *single beam* cantilevers can be calculated, assuming levers of constant thickness, based on measured cantilever dimensions, and even though the suppliers state nominal spring constants, experimental calibration of the spring constant for surface normal deflection  $k_N$  is necessary.

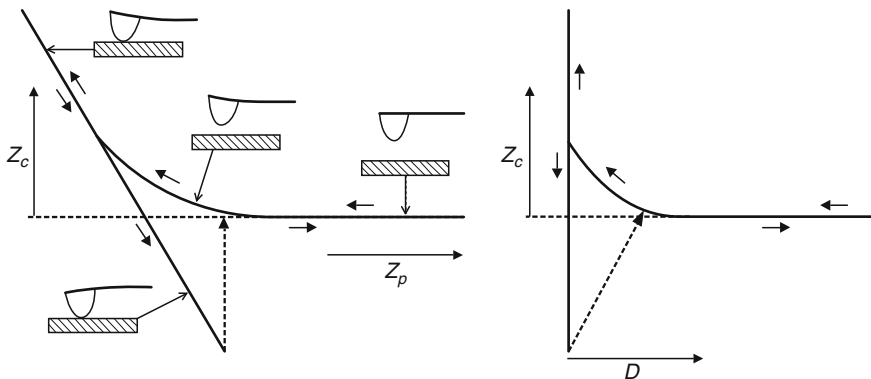


**Fig. 2.29** Schematic of a typical cantilever deflection-vs.-piezo height ( $Z_c$ -vs.- $Z_p$ ) curve (left) and corresponding  $Z_c$ -vs.- $D$  plot, with  $D = Z_c + Z_p$ . Reprinted with permission from [16]. Copyright 2005. Elsevier

The most widely used method, as has been proposed by Hutter and Bechhofer, exploits a measurement of the thermal noise of the cantilever. In the model of a harmonic oscillator, the cantilever spring constant  $k_N$  is inversely proportional to the mean square deflection due to thermal fluctuations (2.4). In practice, a noise spectrum of the deflection amplitude is recorded after the calibration of the deflection sensitivity. This can be manually done for instruments of some AFM brands by “engaging” in CM using false engagement, (see Sect. 3.2 in Chap. 3), and recording a deflection image. The power spectral density of this image is analyzed. The spectrum shows a peak at the resonance frequency, corresponding to the first vibrational mode. This peak is fitted with a Lorentzian curve and the mean square deflection of the first peak is obtained by integration. Nowadays, the thermal noise calibration method is implemented in modern commercial AFMs; thus these laborious steps and fitting can be circumvented (for details compare AFM manuals).

$$\frac{1}{2}k_c\langle\Delta Z_c^2\rangle = \frac{1}{2}k_bT \Rightarrow k_c = \frac{k_bT}{\langle\Delta Z_c^2\rangle}. \quad (2.4)$$

As discussed in detail in [16], the appropriate estimation relies on (2.5), in which the effective deflection  $Z^*$  (the deflection is read from the instrument after determining the sensitivity from the contact part of a force curve on a stiff substrate) and a correction factor  $\beta^*$  are employed that provide the appropriate relation of the (measured) inclination and the (desired) deflection. The appropriate correction factors  $\beta^*$  for rectangular and V-shaped levers are 0.817 and 0.764, respectively. In the actual software, the numerical values may be different, for instance in DI/VEECO systems, the correction factors ( $\chi^2$  correction) should be 1.106 for rectangular and 1.144 for V-shaped cantilevers.

$$k_c = \beta^* \frac{k_bT}{\langle Z_1^{*2}(L) \rangle}. \quad (2.5)$$

An alternative method relies on the acquisition of  $f$ - $d$  curves on (1) a stiff substrate and (2) a reference lever with known spring constant. For this method, the reference lever should have a spring constant close to the one that will be calibrated. If we denote the deflection of the cantilever as  $Z_c$  and the height of the piezoelectric translator as  $Z_p$  (zero is defined for the situation, when the tip just touches the reference cantilever and no deflection has been detected), the spring constant is given by

$$k_N = k_{\text{ref}} \frac{Z_p - Z_c}{Z_c} = k_{\text{ref}} \frac{1 - Z_c/Z_p}{Z_c/Z_p}. \quad (2.6)$$

Since the spring constant of the reference cantilever  $k_{\text{ref}}$  is known,  $k_N$  can be obtained from the measured slope of the force curve  $Z_c/Z_p$  obtained on the reference cantilever in the contact regime (Fig. 2.30).

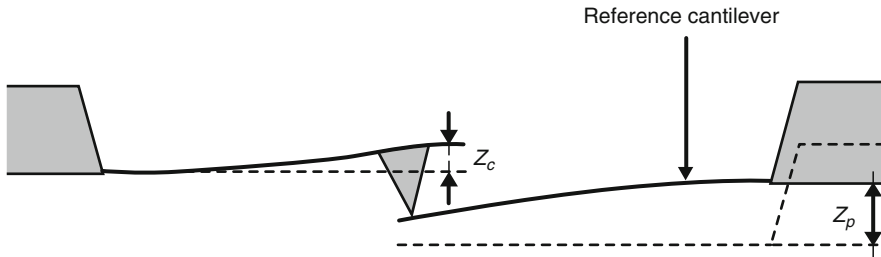


**Fig. 2.30** Schematic of cantilever calibration on reference lever. Reprinted with permission from [16]. Copyright 2005. Elsevier

With calibrated detection system and cantilevers at hand, the measurement of adhesive forces can be carried out as outlined in Chap. 4.

By contrast, the calibration of the force constant of a given cantilever and the photodiode sensitivity for measurements of lateral forces remained challenging until recently [17–19]. The conventional calibration techniques proposed for the calibration of LFM can be grouped into (1) reference methods [20] and (2) two-step [8, 21, 22], procedures. The challenges mentioned arise from the fact that the reference methods suffer from systematic errors introduced by contaminations on the reference samples and that a separate calibration of the lateral force constant  $k_L$  and the photodiode sensitivity for lateral deflection  $S_L$  is hampered by a number of problems. The accuracy of the determined value of  $k_L$  is limited because of large errors in the determination of the cantilever dimensions and the uncertainty in the values for Young's moduli and Poisson's ratios for  $\text{Si}_3\text{N}_4$  (if applicable). The unavailability of a reliable in situ method to calibrate the photodiode sensitivity  $S_L$  and its dependence on factors, including laser beam position on the lever, spot size, asymmetry, etc., represent additional complications.

A third group of calibration procedures, the (3) direct (single step) [23–25] techniques avoids (many of) these problems. In particular, the so-called improved wedge-calibration method, in which a tip/cantilever is scanned across a calibration sample with two well-defined slopes (see Fig. 2.31), allows one to calculate the calibration factors with an error of ca. 5% [18].

In the wedge calibration method, a cantilever is scanned across a calibration sample with two well-defined slopes. The friction signal is recorded as a function of the applied load. At a given load  $L$ , friction and normal forces (normal force = load + adhesion  $A$ ) depend on the direction of motion (Fig. 2.32).

It can be shown that relations between measured lateral forces (half width of friction loop  $W = (M_u - M_d)/2$ ) and the friction loop offsets ( $\Delta = (M_u + M_d)/2$ ) for sloped and flat surfaces at a given load (2.7–2.10) can be used to calculate the friction force calibration factor  $\alpha$  [ $nN/V$ ].  $M$  denotes the torsion moment involved, the subscripts  $u$  and  $d$  denote uphill and downhill scan directions, and the subscripts  $s$  and  $f$  denote sloped and flat surfaces, respectively.

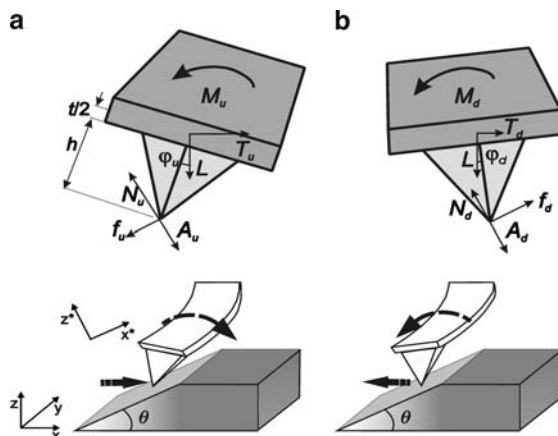


**Fig. 2.31** Schematic illustration of cantilever torsion while (a) sliding up and (b) sliding down on a sloped surface (in the  $x$  direction). While sliding across a sloped surface with angle  $\theta$ , the acting forces (the applied load  $L$ , the horizontal tractive force  $T$ , the adhesion force  $A$ , the reaction force from the surface acting on the tip with a component  $N$  in the surface normal direction and a component  $f$  (friction force) parallel to the surface) and the torsion momentum  $M$  are in equilibrium and depend on the direction of motion – uphill and downhill, denoted here with subscripts  $u$  and  $d$ , respectively.  $\varphi$  represents the torsion angle of the cantilever, which is proportional to the friction force;  $h$  and  $t$  stand for tip height and cantilever thickness, respectively (reproduced with permission from [18]. Copyright 2006 American Chemical Society)

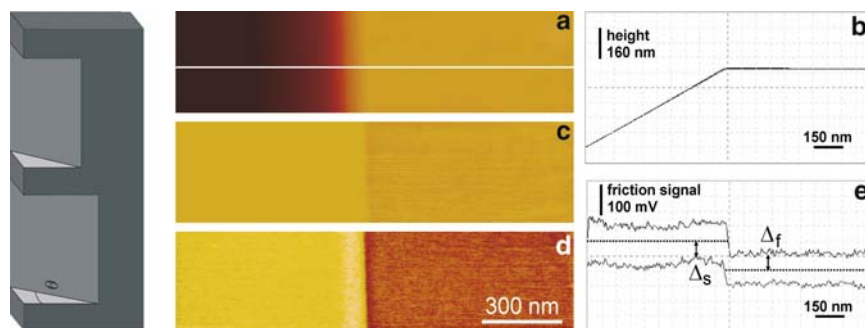


**Fig. 2.32** Left: Schematic of calibration specimen; Right: Example of experimental data measured with a  $\text{Si}_3\text{N}_4$  tip on both sloped and flat surfaces: (a) topography image (vertical scale from black to white 800 nm), (b) cross section of topography (vertical scale 800 nm), (c) difference friction image (trace – retrace, vertical scale 0.5 V), (d) off-set of the friction loops (trace + retrace, vertical scale 0.5 V) and (e) friction loop corresponding to cross section shown in panel (b) (the off-sets for sloped and flat surface,  $\Delta_s$  and  $\Delta_f$ , respectively, have been marked). Reproduced with permission from reference [18]. Copyright 2006. American Chemical Society

$$\frac{\mu_s(L + A \cos \theta)}{\cos^2 \theta - \mu_s^2 \sin^2 \theta} = \alpha W_s \quad (2.7)$$

and

$$\mu_f = \frac{\alpha W_f}{(L + A)} \quad (2.8)$$

$$\frac{\mu_s^2 \sin \theta (L \cos \theta + A) + L \sin \theta \cos \theta}{\cos^2 \theta - \mu_s^2 \sin^2 \theta} = \alpha (\Delta_s - \Delta_f) \quad (2.9)$$

$$\sin \theta (L \cos \theta + A) \cdot \mu_s^2 - \frac{\Delta_s - \Delta_f}{W_s} (L + A \cos \theta) \cdot \mu_s + L \sin \theta \cos \theta = 0. \quad (2.10)$$

By solving the quadratic (2.10) for  $\mu_s$ , two mathematical solutions are provided (for any given load and adhesion). When substituted into (2.7) or (2.8), these yield correspondingly two values of the friction calibration factor  $\alpha$ . As  $\alpha$  must be identical for sloped and flat surfaces, we obtain  $\mu_f$  from (2.8). The physical solution stands for  $\mu_s, \mu_f < 1/\text{tg}\theta$ . A more detailed description of the wedge calibration procedure can be found in [26, 27].

Thus, in practice we record friction data (images or loops) for both trace and retrace for different setpoints. We also acquire and capture for each setpoint the entire  $f$ - $d$  curve to calculate the mean pull-off force (= adhesion  $A$ ) and the load  $L$ . The analysis of the friction data provides the half width of friction loop  $W = (M_u - M_d)/2$  and the friction loop offsets ( $\Delta = (M_u + M_d)/2$ ) for sloped and flat surfaces for each load, i.e., we measured and calculate the following:

$$A; W_{s, \text{load}}; W_{f, \text{load}}; \Delta_{s, \text{load}}; \Delta_{f, \text{load}}.$$

With knowledge of the inclination angle  $\theta$ , we can calculate the friction coefficient  $\mu$  and also the desired calibration factor  $\alpha$  as outlined above.

This direct approach allows one to calculate the calibration factors with an error of  $\sim 5\%$ . As shown, the approach is not affected by an additional small sample tilt, different feedback settings, and a possible tip position off the central cantilever axis. Only laser light interference and nonspherical tip apex shapes must be taken into account. It is pointed out that the laser alignment of each tip used should *not* be altered throughout the experiments, as this would also introduce relative errors. For a more detailed discussion, the reader is referred to [28].

For measurements in liquid, an additional correction factor that corrects the effect of refraction must be considered. By multiplication with the factor  $n_{\text{air}}/n_{\text{liquid}}$  ( $n$ : refractive index) one can conveniently rescale the values of lateral photodiode sensitivity obtained in air ( $S_L^{\text{Air}}$ ) employing, e.g., the improved wedge calibration method using a universal calibration specimen, to obtain the correct value for  $S_L^{\text{Liquid}}$  [29] (Fig. 2.33).

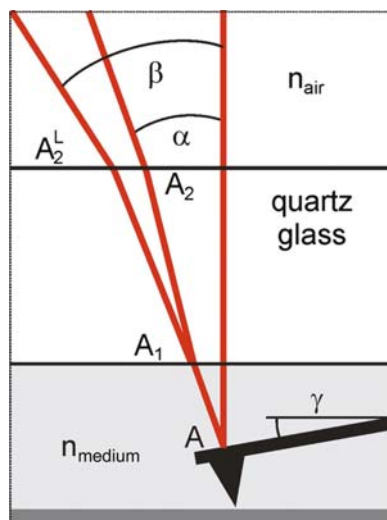


**Fig. 2.33** Schematic of effect of refraction: Upon bending the cantilever by an angle  $\delta$  (not shown in scheme), the light leaves under an increased angle  $\beta = 2\delta^L$ , instead of leaving the liquid cell under an angle  $\alpha = 2\delta$ . Reproduced with permission from [29]. Copyright 2007. American Chemical Society

The situation for tapping mode is somewhat simpler, as the resonance frequency is determined for each cantilever at the beginning of an experiment in the conventional tapping mode tune.

## 2.2.6 General Guidelines for AFM Laboratories

AFM operation requires a minimum of vibrations. These vibrations refer to not only building vibrations, but also vibrations caused by airflow, persons walking in the lab, and equipment, such as personal computers, the AFM controller, etc. To damp out vibrations, AFM scan units are typically placed on passive and/or active vibration damping systems, such as:

Passive: blocks of concrete

Heavy plates suspended from rubber (bungee) cords

Rubber and other antivibration pads

Active: piezo tables

Air tables

Vibrations that are caused by equipment may be transmitted via the corresponding cables. To dampen out vibrations of this sort, cables can be equipped with heavy masses, e.g., metal parts. For sensitive experiments, the placement of the entire AFM scan unit inside acoustic enclosures may be also advisable.

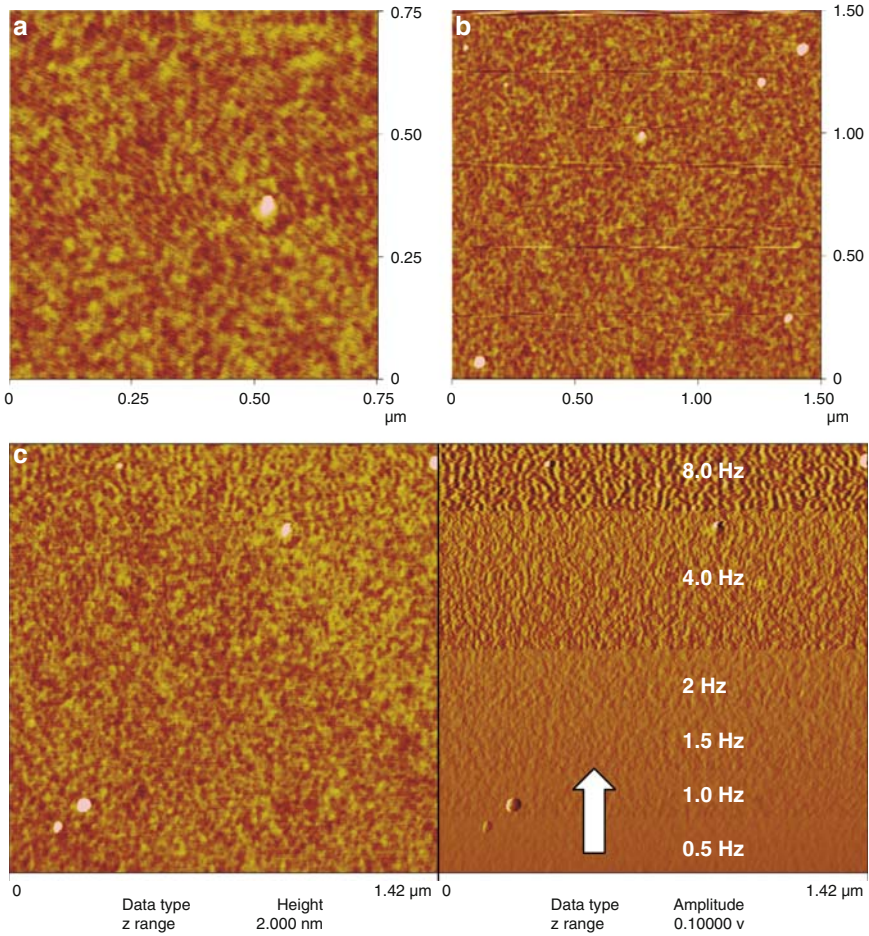


**Fig. 2.34** TM–AFM height images displaying (a) vibration noise due to insufficient vibration isolation and (b) horizontal spikes due to external shocks that were not damped by the isolation system. In *panel (c)* an upscan with six different velocities is displayed

In addition, the temperature should be constant, and humidity should preferably not exceed 65% or fall below 10%.

Above, some AFM images are shown that display typical regularly spaced features that are the consequence of vibrations (Fig. 2.34a); in addition, erroneous scan lines due to shock-like vibrations are depicted in panel (b). In addition to vibrational noise, more or less regular features may appear in the images when the scan velocity is set too high. In panel (c) a dual height and amplitude scan is shown (upscan) in which the scan velocity was stepwise increased. The magnitude of the rms amplitude increases as the feedback loop is more and more unable to correct the encountered topographic changes; for the highest scan rate oscillatory-like features are observed.

### 2.2.7 Data Evaluation

Data evaluation is nearly as important as data acquisition and despite the many good offline options of the various AFM softwares and separate programs, many data published still to date suffer from artefacts introduced in the data processing and evaluation phase. A full account on data treatment, analysis, and evaluation is out of scope of this book; therefore, we will focus on a few selected procedures that are most relevant and can be carried out on most commercial AFM brands *without* other specialized software.

The reader is strongly encouraged to capture and store the data as “raw” as possible, i.e., without planefit, flattening, or filtering. As the data is being altered with most procedures, it is also wise to store processed data in separate files.

Rudimentary data processing is necessary as the captured raw data may suffer from the following shortcomings (reminder: the data displayed on the screen during the AFM scan are already processed data).

One of the problems is the fact that the sample plane and the  $x, y = (0, 0)$  plane of the scanner only rarely coincide, hence part of the image is well visible while other parts are above or below the plane displayed. Depending on the level of mismatch, a planefit (first order) levels the image. Higher order planefits remove artefacts related to scanner bow effects. To perform an appropriate planefit, it may be necessary to *include only* certain areas in the calculation of the mean plane. This is the case if large-scale corrugations on a flat film are present that do not reside in the mean plane.

The planefit procedure calculates a single polynomial fit for the entire image and then subtracts the polynomial fit from the image. One differentiates different order of planefitting:

First order planefit removes tilt;

Second order planefit removes tilt and an “arch-shaped” bow;

Third order planefit removes tilt and an “S-shaped” bow.

A second issue is a mismatch between certain scan lines due to various effects, including vertical ( $Z$ ) scanner drift, image bow, and skips. This effect can be eliminated by the operation called flattening. A first order flattening is a similar operation to the line by line planefit described in Sect. 2.1.1.

Zero order (0) flattening removes the  $Z$  offset between each scan line by subtracting the average  $Z$  value from every point in the scan line;

First order (1) flattening removes the  $Z$  offset between scan lines, and the tilt in each scan line;

Second order (2) flattening removes the  $Z$  offset between scan lines, and the tilt and bow (arch shaped) in each scan line.

Third order (3) flattening removes the  $Z$  offset between scan lines, and the tilt and bow (S-shaped) in each scan line.

Filtering, such as high pass or low pass filtering, is *not* advisable, unless high resolution imaging is performed and some (e.g., vibrational) noise should be eliminated. Under certain circumstances these filtering operations can indeed alter the vertical scale, which is not wanted.

### 2.2.7.1 Example: Determination of the Film Thickness of Spin-Coated Films

A spin-coated poly(methyl methacrylate) (PMMA) film on silicon has been scratched using sharp tweezers. This procedure removes the film, but does not damage the underlying silicon wafer. The raw AFM height data are shown in Fig. 2.35a. From the image, it is clear that the sample plane was not exactly horizontal; therefore, a plane fit operation was performed. In Fig. 2.35b, we display a zero order plane fit, which only moves the center of the image to the zero plane. In Fig. 2.35c, the result of a first order plane fit is shown that was done considering the

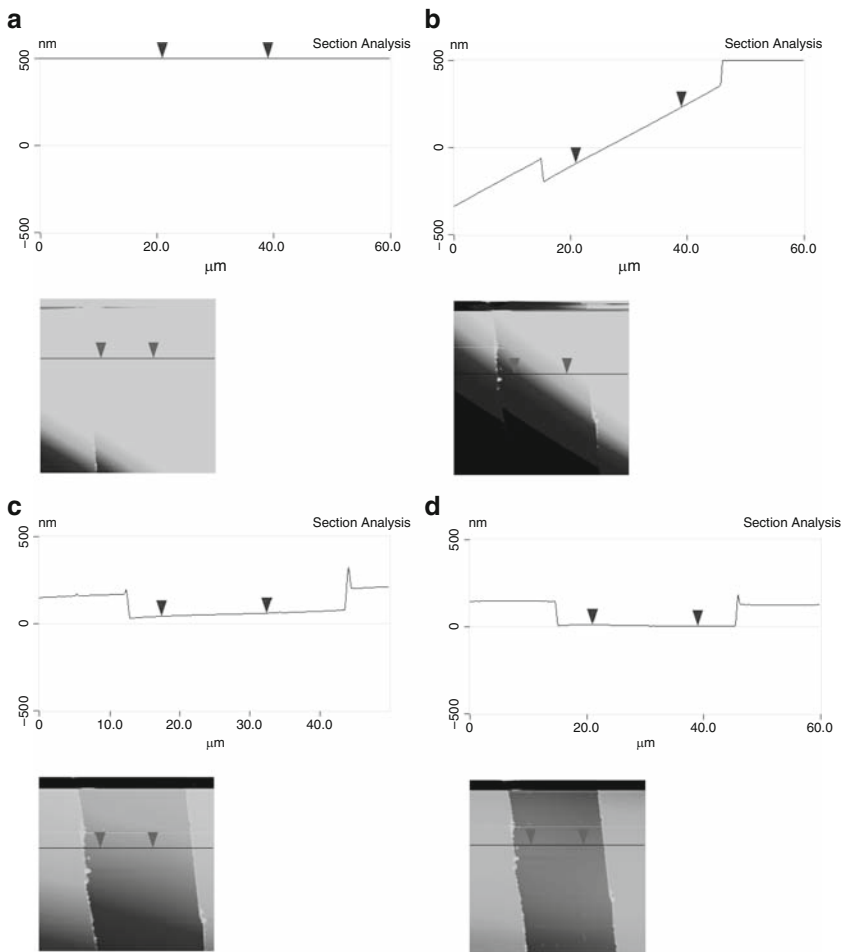


**Fig. 2.35** AFM height images and corresponding cross sectional analyses of a PMMA thin film on silicon that was partially removed in the vertical direction (**a**: raw data; **b–d** plane-fitted data, details see text)

entire scanned image, while in Fig. 2.35d only the areas of the film, but not of the silicon wafer were considered.

The cross sections show the sample tilt (panel b) and the inadequately calculated planefit in panel (c). The clearly discernible slope in the direction of the section analysis may cause errors in height measurements that in turn may lead to erroneous thickness values. Only the data shown in panel (d) displays a cross section with no discernible slope, as would be expected for the sample.

### 2.2.7.2 Appropriate Flattening

If a flattening is necessary, it must be properly executed: high and low features must be excluded from the analysis (see corresponding software manuals for exact procedures). In Fig. 2.36, an AFM height image of a calibration grating is shown, in which parts of the square shaped depressions were excluded from the calculation (as is advised). In the lower two rows, this has not been done on purpose. As a result, a vertical profile would show elevated areas between the depressions that are an artefact of the data processing.

In the examples discussed above, we have already utilized a common data display format, i.e., the top-view. In this option, the height information is displayed in a color (or gray scale) scheme. Typically the z scale is shown with exaggerated zoom; in the figures shown above the z-scale covers over the entire range height values from 0 to 1000 nm over a lateral scan size of  $(60 \mu\text{m})^2$ . In addition, the color scale and contrast settings may enhance the subjective contrast and particular

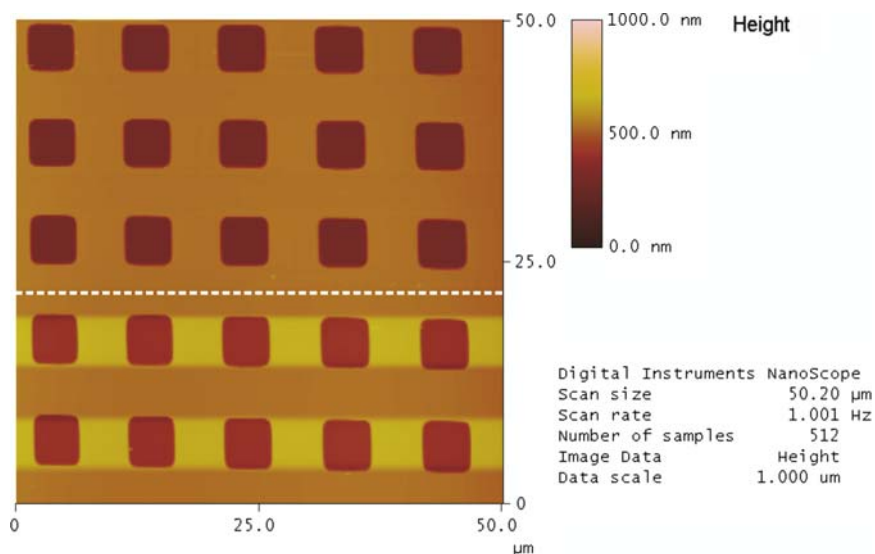


**Fig. 2.36** AFM height image in which the *upper part of the image* was properly flattened, while for the *lower parts* the depressions were not excluded from the analysis. The calibration grating is of course devoid of elevated squares (compare also Fig. 2.28a)

features, while small-scale variations in slope for instance may be hidden within one type of gray scale that is without contrast to the eye. Hence, a careful cross-sectional analysis (compare Fig. 2.35) is advisable.

### 2.2.7.3 Data Display Formats

The data can also be displayed as a 3D plot. Again, the height information is shown with exaggerated scale. The different display formats and the dependence of the “visual appearance” and appeal on the color and contrast settings are exemplified in Fig. 2.37, where the same data (polymeric colloidal particles on a flat silicon wafer) are shown with different  $z$ -scales and contrast settings.

### 2.2.7.4 Data Analysis Tools

Some of the most important data analysis tools are shown for an image of a microphase separated block copolymer film. The tapping mode AFM height data were subjected to a first order plane fit to eliminate the effect of sample tilt (Fig. 2.38).

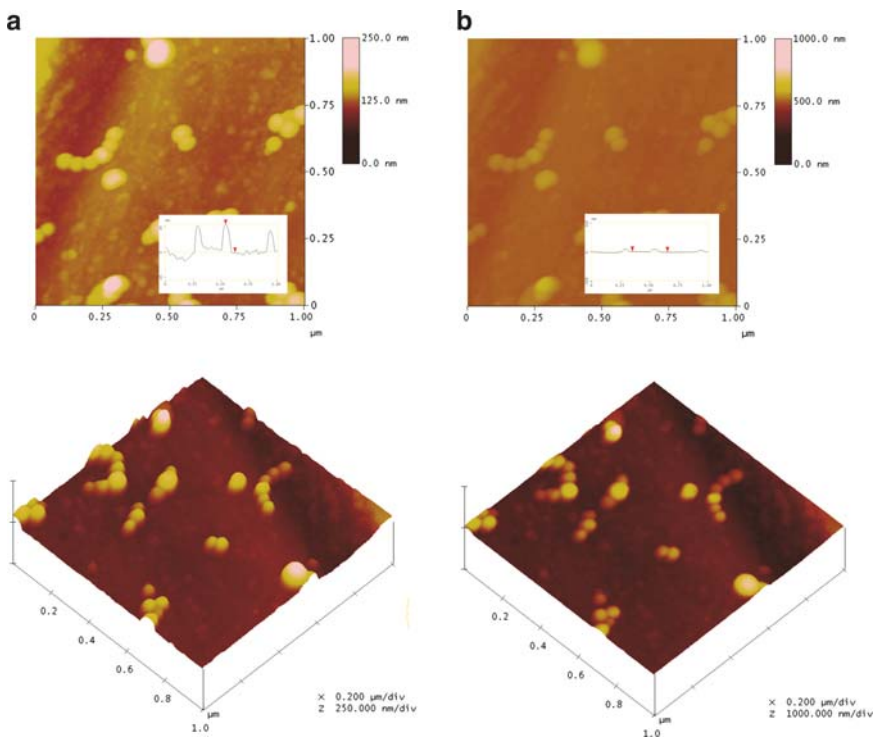


**Fig. 2.37** The same AFM height data of colloidal particles displayed with different scales and settings. In *panel (b)* the lateral and vertical scales match

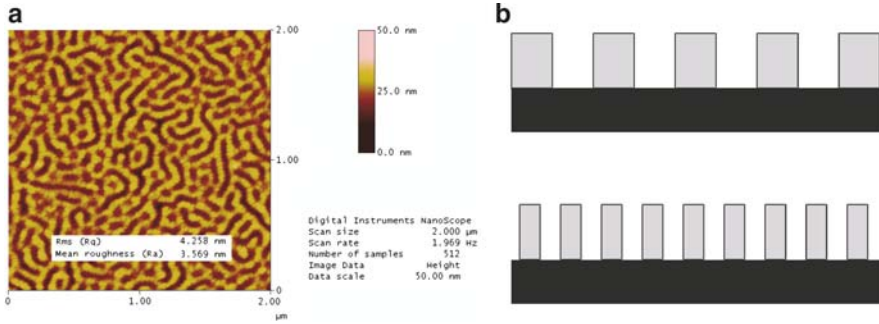


**Fig. 2.38** (a) TM–AFM height image of block copolymer and calculated  $R_q$  and  $R_A$  roughness values. The displayed numbers (output of software) possess an unjustified number of decimals. (b) Schematic of two surface profiles that exhibit identical  $R_q$  and  $R_A$ , yet widely different feature size

### 2.2.7.5 Roughness

The roughness of sample surfaces is often of interest. Different roughness parameters can be calculated based on the acquired AFM data. Most often the *rms* roughness  $R_{\text{rms}}$  (also denoted  $R_q$ ) is calculated as the standard deviation of all pixel values from the mean pixel value  $\bar{Z}$ .

$$R_{\text{rms}} = \sqrt{\frac{\sum_{\substack{x=1,N \\ y=1,M}} (Z_{x,y} - \bar{Z})^2}{(N-1)(M-1)}}. \quad (2.11)$$

The  $R_A$  roughness value represents the standard deviation of pixel value from the mean plane.

$$R_A = \sqrt{\frac{\sum_{\substack{x=1,N \\ y=1,M}} (Z_{x,y} - \bar{Z}_{x,y})^2}{(N-1)(M-1)}}, \quad (2.12)$$

where  $N$  and  $M$  are the number of pixels in the  $x$  and  $y$  directions, and  $Z_{x,y}$  is the image pixel height with respect to the center plane height  $\bar{Z}_{x,y}$  for the pixel  $(x, y)$ .

These and other roughness parameters are discussed in [30]. Caution has to be exercised when comparing roughness data. According to (2.11) and (2.12), the two surfaces shown schematically in Fig. 2.38b possess identical roughness values.

### 2.2.7.6 Profile (Cross section)

Cross-sectional plots and profiles, as already utilized in many instances above, are very useful to analyze horizontal or surface distances, as well as step heights and

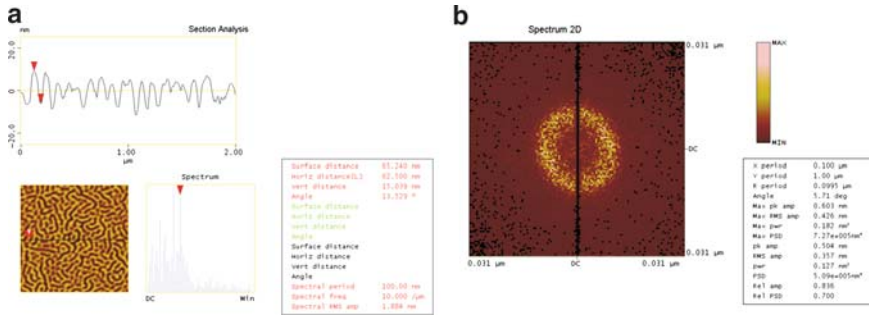


**Fig. 2.39** (a) Cross sectional analysis of AFM data incl. 1D-FFT analysis along the selected line. (b) the 2D-FFT shows the typical periodicity in 2D; the  $R$  value agrees well with the value obtained from the 1D analysis in *panel (a)*

periodicities along one particular line (via a 1D fast Fourier transform (FFT) spectrum). As shown, the corrugation and spacings in a block copolymer film can be directly analyzed. In addition, the spectral period of the 1D-FFT reveals the typical repeat distance along the depicted line. In panel (b), the 2D-FFT that is calculated in a separate analysis, is also shown (Fig. 2.39).

### 2.2.7.7 Step Height Analysis

The determination of film thicknesses can be carried out, as shown above, by analyzing cross sectional plots. An improved statistics is obtained using a step height analysis. Here, two sets of two lines define certain areas on the two levels of altitude, which are analyzed. Instead of calculating individual height differences, the software estimates the mean difference in height between the areas selected Fig. 2.40.

### 2.2.7.8 Bearing Analysis

In the bearing analysis, the depths of all pixels of the image with respect to a reference point, e.g., the highest pixel are analyzed. This type of analysis renders the estimation of surface coverages and the estimation of depths possible, either for the entire image or for a selected area. The depth distribution of pixels may for instance reveal the depth levels present. In case of the calibration grating shown in Fig. 2.28a, this would be a bimodal distribution (Fig. 2.41). These data can be deconvoluted using graphics analysis software, similar to a spectroscopic deconvolution. The cumulative distribution depicted on the right hand side aids in the estimation of surface coverage.

There are of course numerous other analysis methods, including grain size, localized depth analyses, etc. The reader is referred to the manuals of the AFM software and to the Appendix for independent analysis software packages.

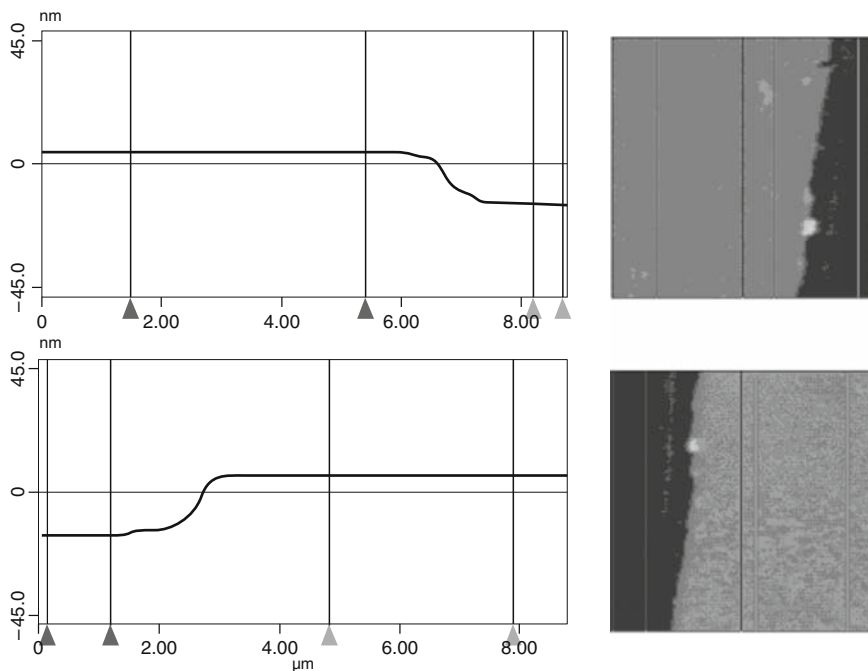


**Fig. 2.40** Step height analysis of AFM height images of a thin polymer film prior to and after swelling (step heights of 19.0 and 21.3 nm were measured). Reproduced with permission from [31]. Copyright 2005. American Chemical Society

### 2.2.8 Typical AFM Artefacts

The possible presence of artefacts in microscopy data is an important aspect, which always has to be taken into account when analyzing the images. “Seeing is believing” is a corollary of the quick, and sometimes over-quick, jump from visual impression to interpretation. Optical illusions are well known to everyone; still no one would question the ability of our visual system to differentiate different objects. In microscopy, however, and AFM and related techniques in particular, the presence of artefacts has led to some reservation to accept the techniques as characterization and analytical techniques, and even brought discredit to the technique(s) in general. This may in parts be attributed to uncritical authors who made or make unsubstantiated claims. However, another part may be due to researchers and readers who shy away from appropriate interpretation of the data; appropriate in the sense of established characterization techniques such as nuclear magnetic resonance (NMR). If the imaging mode, the nature, and extent of tip-sample interactions, as well as possible artefacts, are taken into consideration, and if the instrument and detection scheme are properly calibrated, AFM becomes a reliable *quantitative* surface analysis technique.

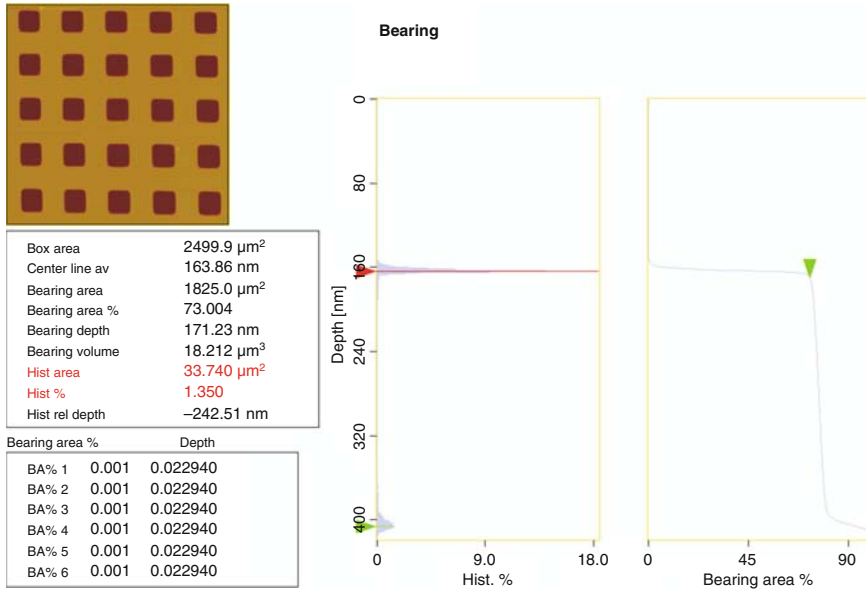


**Fig. 2.41** Bearing analysis of AFM height image of calibration grating displaying the depth distribution (*middle*) and the cumulative distribution of depths (*right*)

One limitation of AFM is of course the fact that the data acquired is convoluted with information of the probe tip (size, asymmetry etc.). This phenomenon is called “tip imaging.” Strictly speaking all AFM images show this effect, albeit to a different extent. In the philosophical limit of an atomically sharp tip with infinite aspect ratio, the data are not convoluted unless we image single atoms. Depending on the size and geometry of the tip, features appear broader than they are in reality (Fig. 2.42a). In a very simplified model, assuming spherical tip apex and a spherical object, it can be shown how the width is overestimated. Assuming or determining the actual tip shape and dimensions can thus be helpful to deconvolute the data. Typical tip radii are anywhere between a few to several tens of nanometers; thus, for smaller objects and features, this effect must be taken into account. For instance, the individual dendrimers shown in Fig. 2.42b are substantially overestimated in width.

For very high and narrow features it may happen that the image contains practically no information on the objects that was imaged. A mirror image of the tip is observed. As shown in, this is the underlying principle of tip calibration using a standard (Fig. 2.43).

While the tip images, as shown above, do not occur too frequently, unless very rough surfaces are imaged or samples are contaminated, more subtle effects occur very well. In the case of an asymmetry of the probe tip, this is readily recognized, as all “tip images” possess the same orientation. Changing the scan angle does not help to differentiate this kind of artefact from true features, as the actual orientation does not change; only the relative one does change. Thus, the features would all rotate as

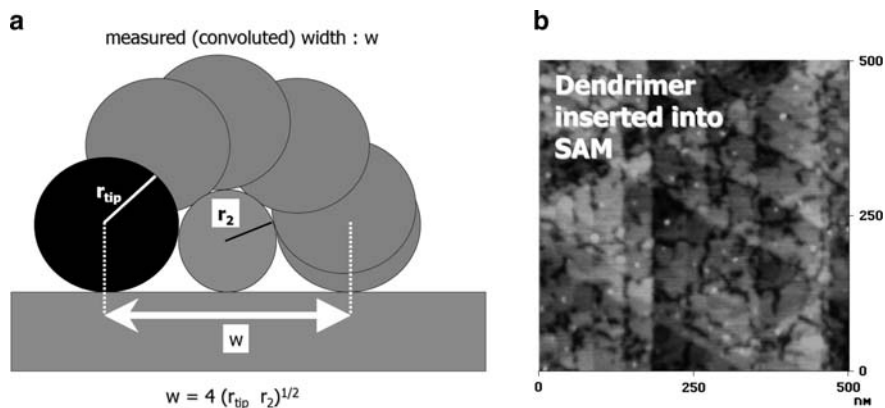


**Fig. 2.42** (a) Model to quantitatively describe the effect of tip broadening; (b) TM AFM height image of dendrimers; while the diameter of dendrimers in solution was determined to be  $\sim 3.5$  nm the dimension of each “dot” are: height  $0.9 \pm 0.2$  nm, width  $23 \pm 4$  nm). Reproduced with permission from [32]. Copyright 2000. American Chemical Society

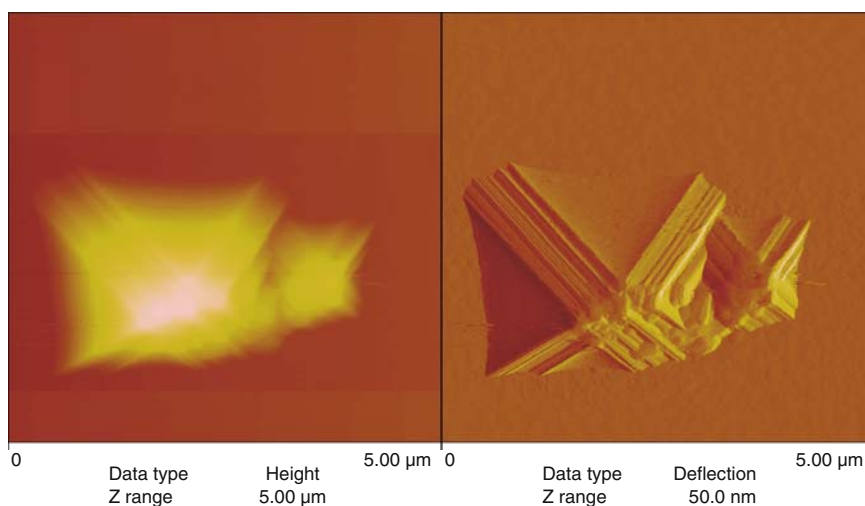


**Fig. 2.43** Contact mode AFM and deflection images exhibiting a tip artefact

would the image. To be able to decide whether the triangular features in Fig. 2.44 are real, one would need to manually rotate the specimen relative to the tip.

Similarly clear is the presence of a so-called “double tip” (Fig. 2.45a). Here, the tip exposes two points (sometime in different levels). Again, the features possess typical orientations, as demonstrated nicely below for electrospun polymer fibers (Fig. 2.45). The fibers appear to be double, depending on their orientation. Since two fibers are apparently visible when they are oriented horizontally, while these fibers

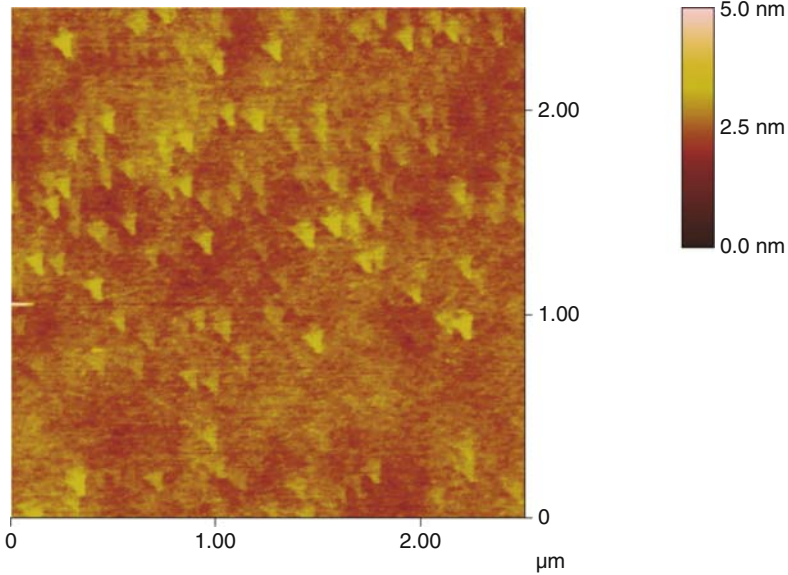


**Fig. 2.44** Contact mode AFM image displaying a tip artefact

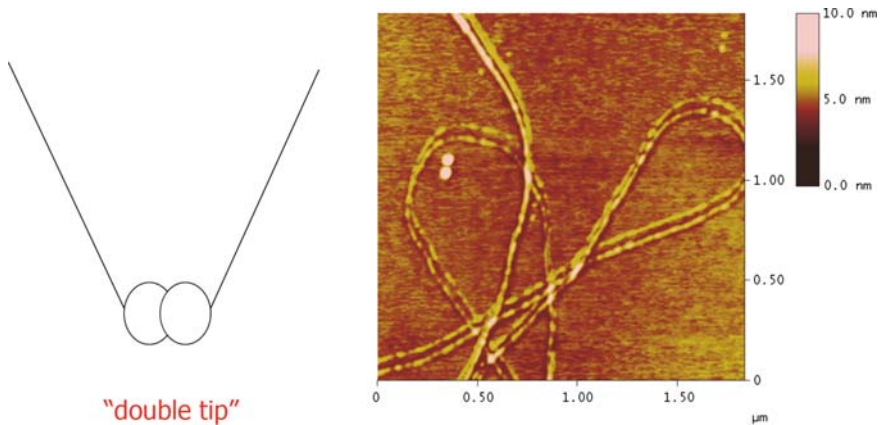


**Fig. 2.45** (a) Schematic of a double tip; (b) AFM height image of electrospun polymer fibers. The appearance of parallel fibers (i.e., a pair of fibers) is highly unlikely on the basis of the orientation dependence of the pairs

seems to merge to one for vertical orientation, the double tip must possess two points that are aligned along the vertical direction.

More difficult is the differentiation of tip convolution effects if there is no hidden symmetry. In the images shown in Fig. 2.46, the tip was altered in the course of an experiment. In fact, the images show the same area of a vertically stretched

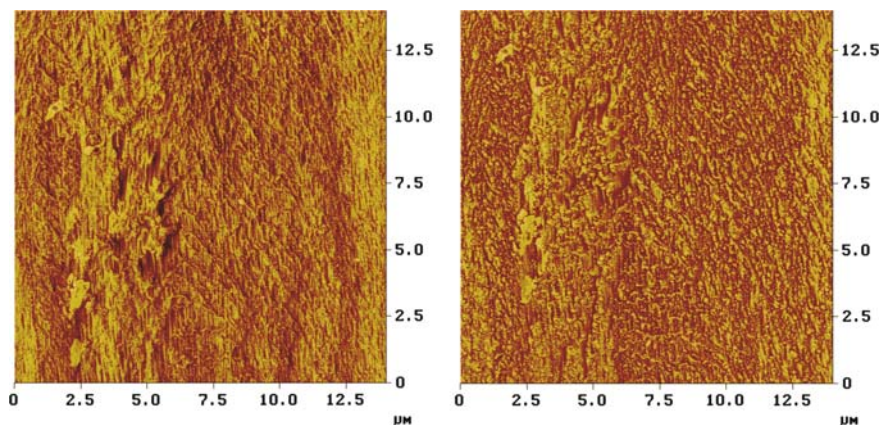


**Fig. 2.46** TM–AFM images of the same area of a vertically stretched elastomeric polypropylene as imaged (a) with a fresh and (b) with an aged tip [33]

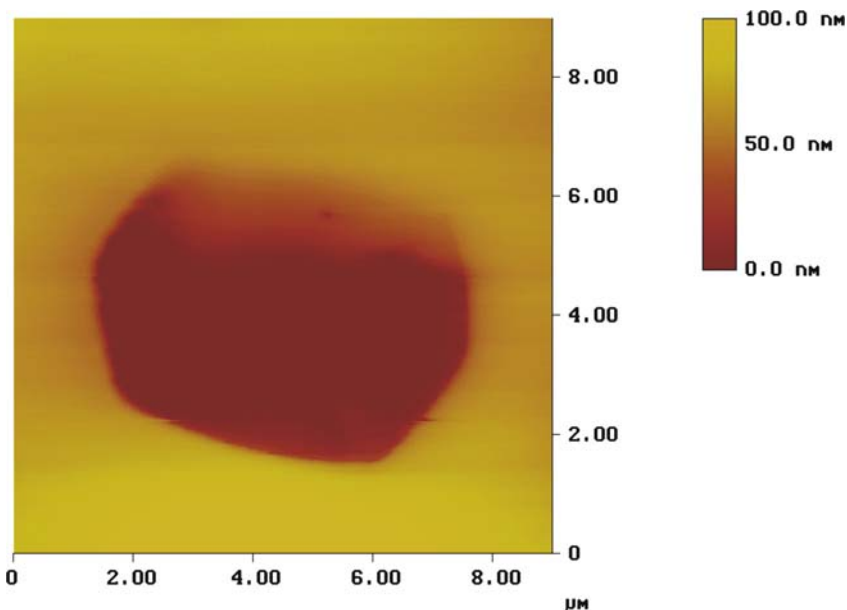


**Fig. 2.47** TM–AFM image of a PEO crystal in a melt of PEO. Because of an imaging artefact the crystal appears to be located at a lower depth (Reproduced with permission from [34]. Copyright 2003. American Chemical Society)

elastomeric polypropylene as imaged (a) with a fresh tip and (b) with a likely damaged (broken) or contaminated (by particulates) tip. The images suggest a fibrillar and a grainy texture, respectively.

From these examples, it becomes clear that consistent data acquired with a number of probes may be indeed required to confirm certain results.

Additional important artifacts are related to the effect of the probe tip on the sample specimen. The scanning tip, especially in CM, may result in plastic modification (recognized as vertical ridges (compare Sect. 3.2.3 in Chap. 3; Fig. 3.16). For any experiment, it is hence advisable to zoom out to a larger scan area once in a while to check whether or not the tip has modified the previously scanned area. This can be seen either as altered texture and morphology or as friction or phase images (if applicable).

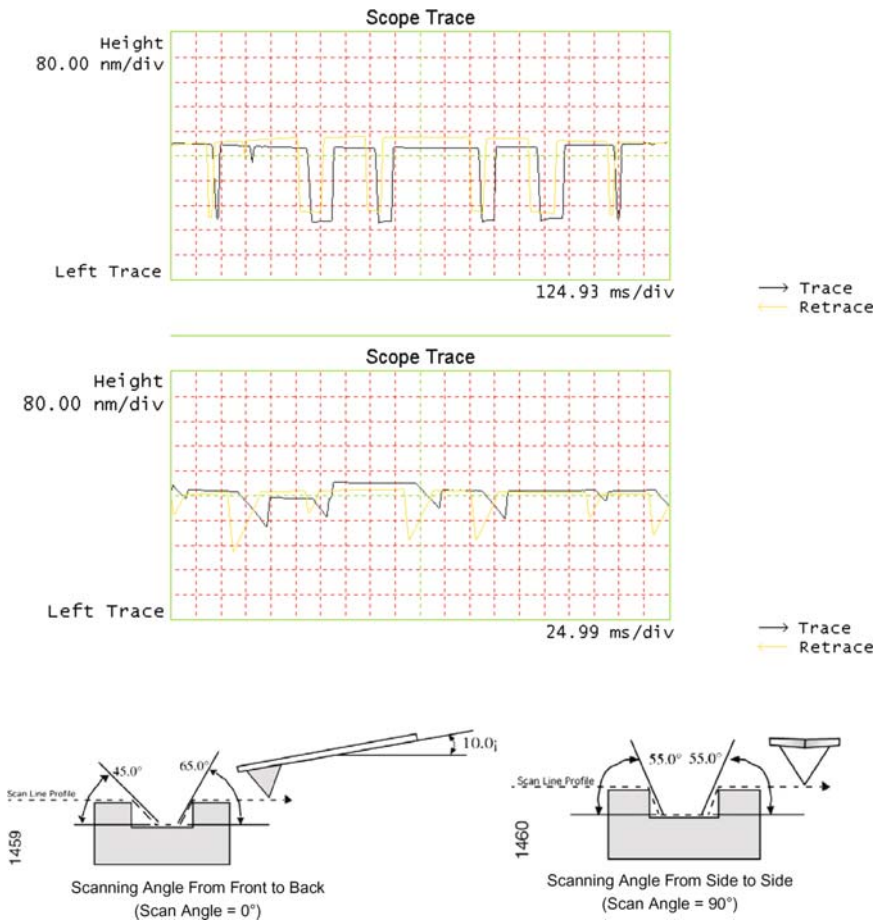


**Fig. 2.48** Scope traces (TM–AFM) with high (*upper panel*) and too low (*middle panel*) gains. The mounting angle of the AFM cantilever and the inclination angle of the tip on the cantilever determine the possibility to image steep features, as shown for a silicon nitride CM AFM probe in the *bottom panel* (reproduced with kind permission from the Veeco user manual). As a result of this, the tip’s interaction with sidewalls may depend on the direction

The height data obtained depend, as mentioned before, on the quality of the feedback loop (gain setting). In addition, it should not be overlooked that the tip may compress softer areas more than stiffer areas leading to an underestimate of height for the former areas. In tapping mode, the damping may be more pronounced on a soft, sticky, or highly energy dissipative material in some area, thus resulting in an overestimate of the height of these areas with respect to others. An extreme example (not typically observed) is shown in Fig. 2.47, where a poly(ethylene oxide) lamellar crystal has been imaged in the melt. The melt damps the oscillation of the tip/cantilever assembly to such an extent that the melt appears to be at a higher altitude than the crystal (independent images after complete crystallization confirm that the crystal is *not* located inside the melt).

Other artefacts refer to improper scanning conditions and include a halo in the fast scan direction after traversing higher features. If the gains are too low or/and the scan velocity is too high, the tip does not track the surface profile adequately. A comparison of trace and retrace scan (these should overlay well) helps to identify this artefact (Fig. 2.48). The top panel shows the scope trace for an AFM scan of a topographic structure with appropriate gains. The scanner calibration is not optimal as there are (1) a clearly discernible bow and (2) a substantial scan line offset (trace and retrace appear to be shifted). The issue is, however, that in the middle panel the tip did not trace the surface appropriately, as the gains were too low.

Vanishing contrast may be caused by selecting a setpoint that is almost equal to the differential signal for the undeflected cantilever and equal to the *rms* amplitude of the freely oscillating forced oscillator for CM and TM, respectively.

Thermal or instrumental drift (e.g., due to scanner creep in open loop configurations) is a problem that leads to elongated features. As drift is a vectorial quantity (shifted length over time in a given direction) its distorting impact on the image

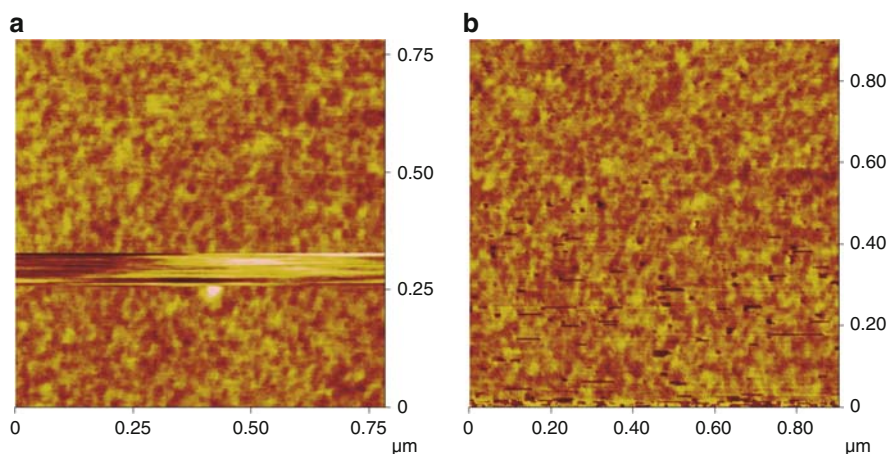


**Fig. 2.49** Overview on artefacts in TM-AFM: (a) TM-AFM height image of a scan during which the tip temporarily lost contact with the sample surface (setpoint  $\sim$  free oscillation amplitude); panel (b) displays the bistability effect in intermittent contact mode AFM

depends on relative scan angle and scan velocity. The absence of drift is confirmed if images are captured with disabled slow scan axis (here the scan lines of nominally one and the same line are added on top of each other). Vertical lines indicate the absence of drift; this procedure should be carried out for two different scan angles as the drift direction may coincide with the vertical direction for one angle.

In friction force microscopy, laser light interference may lead to artefacts that are often eliminated by subtracting trace and retrace (after scan line shift correction).

Finally, missing scan lines due to electronic noise, the tip not tracing the surface properly, or the mentioned bistability (in tapping mode, see Chap. 1) may appear. In the later case, one should change the setpoint or the absolute amplitude to exit the region of bistability, while the former line can be removed electronically afterwards (Fig. 2.49).

## References

1. Schönherr H (1999) From functional group ensembles to single molecules: scanning force microscopy of supramolecular and polymeric systems. Ph. D. Thesis, University of Twente
2. Magonov SN, Elings V, Whangbo M-H (1997) *Surf Sci* 375:L385–L391
3. Snetivy D, Vancso GJ (1993) *Langmuir* 9:2253–2254
4. Landau LD, Lifshitz EM (1986) *Theory of elasticity*, vol 7. Pergamon, Oxford
5. Albrecht TR, Akamine S, Carver TE, Quate CF (1990) *J Vac Sci Technol A Vac Surf Films* 8:3386–3396
6. For V-shaped or triangular levers different approximations exist, e.g. the parallel beam approximation: Sader JE (1995) *Rev Sci Instrum* 66:4583–4587
7. The values of Young's modulus in the [100], [110] and [111] directions are  $E_{[100]} = 130$  GPa,  $E_{[110]} = 168$  GPa, and  $E_{[111]} = 187$  GPa, respectively. Wortman JJ, Evans RA (1965) *J Appl Phys* 36:153–156
8. Noy A, Frisbie CD, Rozsnyai LF, Wrighton MS, Lieber CMJ (1995) *Am Chem Soc* 117:7943–7951
9. Kiewewetter L, Zhang JM, Houdeau D, Steckenborn A (1992) *Sens Actuator A Phys* 35:153–159
10. Schneider D, Tucker MD (1996) *Thin Solid Films* 291:305–311
11. Levy R, Maaloum M (2002) *Nanotechnology* 13:33–37
12. Ma HL, Jimenez J, Rajagopalan R (2000) *Langmuir* 16:2254–2261
13. Butt HJ, Jaschke M (1995) *Nanotechnology* 6:1–7
14. Tortonese M, Kirk M (1997) *Proc SPIE* 3009:53–60
15. Cleveland JP, Manne S, Bocek D, Hansma PK (1993) *Rev Sci Instrum* 64:403–405
16. Butt HJ, Cappella B, Kappl M (2005) *Surf Sci Rep* 59:151–152
17. Attard P, Pettersson T, Rutland MW (2006) *Rev Sci Instrum* 77:116110
18. Tocha E, Schönherr H, Vancso GJ (2006) *Langmuir* 22:2340–2350
19. Pettersson T, Nordgren N, Rutland MW, Feiler A (2007) *Rev Sci Instrum* 78:093702

20. Buenviaje CK, Ge SR, Rafailovich MH, Overney RM (1998) *Mater Res Soc Symp Proc* 522:187–192
21. Schwarz UD, Köster P, Wiesendanger R (1996) *Rev Sci Instrum* 67:2560–2567
22. Liu E, Blanpain B, Celis JP (1996) *Wear* 192:141–150
23. Feiler A, Attard P, Larson I (2000) *Rev Sci Instrum* 71:2746–2750
24. Ogletree DF, Carpick RW, Salmeron M (1996) *Rev Sci Instrum* 67:3298–3306
25. Varenberg M, Etsion I, Halperin G (2003) *Rev Sci Instrum* 74:3362–3367
26. Ogletree DF, Carpick RW, Salmeron M (1996) *Rev Sci Instrum* 67:3298
27. Varenberg M, Etsion I, Halperin G (2003) *Rev Sci Instrum* 74:3362
28. Tocha E, Schönherr H, Vancso GJ (2006) *Langmuir* 22:2340–2350
29. Tocha E, Song J, Schönherr H, Vancso GJ (2007) *Langmuir* 23:7078–7082
30. Thomas TR (1999) *Rough surfaces*, 2nd edn. Imperial College Press, London
31. Feng CL, Zhang Z, Förch R, Knoll W, Vancso GJ, Schönherr H (2005) *Biomacromolecules* 6:3243–3251
32. Friggeri A, Schönherr H, van Manen H-J, Huisman B-H, Vancso GJ, Huskens J, van Veggel FCJM, Reinhoudt DN (2000) *Langmuir* 16:7757–7763
33. Schönherr H, Wiyatno W, Frank CW, Waymouth RM unpublished data
34. Schönherr H, Frank CW (2003) *Macromolecules* 36:1199–1208

## General Reading

- Binnig G, Quate CF, Gerber C (1986) *Phys Rev Lett* 56:930
- Sarid D (1991) *Scanning force microscopy, with applications to electric, magnetic and atomic forces*. Oxford University Press, Oxford
- Wiesendanger R (1994) *Scanning probe microscopy and spectroscopy, methods and applications*. Cambridge University Press, Cambridge, UK
- Miles MJ (1994) In: Spels SJ (ed) *Characterization of solid polymers*, Chap. 2. Chapman and Hall, New York, pp 17–55
- Goh MC (1995) In: Prigogine I, Rice SA (eds) *Advances in chemical physics*, vol XCI. Wiley, New York
- Sawyer LC, Grubb DT, Meyers GF (2008) *Polymer microscopy: characterization and evaluation of materials*, 3rd edn. Springer, Berlin
- Magonov SN, Whangbo M-H (1996) *Surface analysis with STM and AFM*. VCH, Weinheim
- Colton RJ, Engel A, Frommer JE, Gaub HE, Gewirth AA, Guckenberger R, Rabe J, Heckl WM, Parkinson B (1998) *Procedures in scanning probe microscopies*. Wiley, New York
- Meyer E, Overney RM, Dransfeld K, Gyalog T (1998) *Nanoscience: friction and rheology on the nanometer scale*. World Scientific, Singapore
- Magonov SN, Reneker DH (1997) *Annu Rev Mater Sci* 27:175
- Tsukruk VV, Reneker DH (1995) *Polymer* 36:1791
- Sheiko SS (2000) *Adv Polym Sci* 151:61

- Schiraldi DA, Poler JC (2002) In: Mark HF, Bikales N, Overberger CG, Menges G, Kroschwitz JI, (eds) Encyclopedia of polymer science and technology, vol 1, 3rd edn. Wiley, New York
- García R, Pérez R (2002) Surf Sci Rep 47:197
- Schönherr H (2004) Scanning force microscopy. In: Mark HF, Bikales N, Overberger CG, Menges G, Kroschwitz JI, (eds) Encyclopedia of polymer science and technology, Wiley, New York (doi: 10.1002/0471440264.pst500)



<http://www.springer.com/978-3-642-01230-3>

Scanning Force Microscopy of Polymers

Vancso, G.J.; Schönherr, H.

2010, XIV, 248p. 300 illus., 150 illus. in color., Hardcover

ISBN: 978-3-642-01230-3